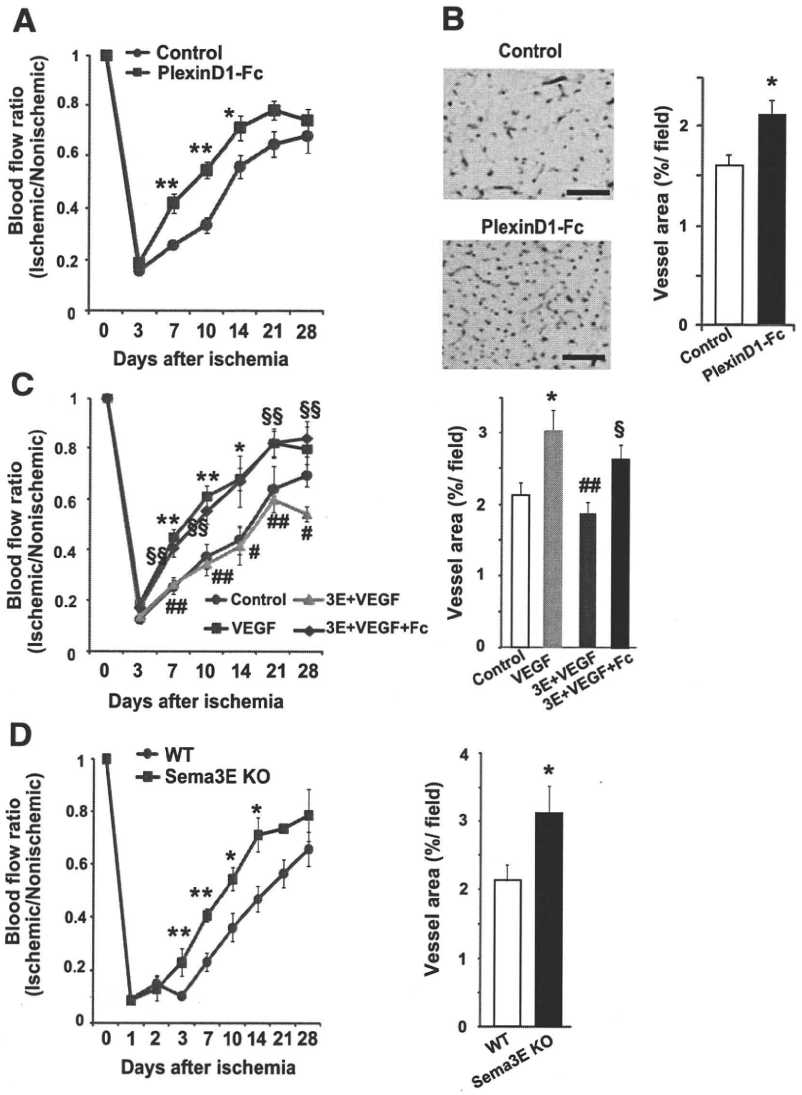

Figure 3. Sema3E negatively regulates angiogenesis in ischemic tissue. A and B, Ischemic limbs of mice were treated with an empty vector (control) or the plexinD1-Fc expression vector (plexinD1-Fc) by intramuscular injection, and blood flow recovery (A) and vessel area (B) were analyzed by laser Doppler perfusion imaging and immunohistochemistry for CD31, respectively. Mice treated with plexinD1-Fc showed better blood flow recovery and a larger vessel area. *$P<0.05$, **$P<0.01$ vs control (n=8 for A and B). Data represent means±SEM. Photographs show immunohistochemistry for CD31 in ischemic limbs on 10 days after surgery. Scale bar=100 μm. C, Ischemic limbs of mice were treated with mock (control), the VEGF vector only (VEGF), the Sema3E and VEGF vectors (3E+VEGF), or the Sema3E, VEGF, and plexinD1-Fc vectors (3E+VEGF+Fc), and blood flow recovery (left) and vessel area (right) were analyzed by laser Doppler perfusion imaging and CD31 immunohistochemistry, respectively. Injection of the Sema3E vector into ischemic limbs suppressed VEGF-induced neovascularization, which was effectively reversed by the plexinD1-Fc vector treatment. *$P<0.05$, **$P<0.01$ vs control; #$P<0.05$, ##$P<0.01$ vs VEGF; §$P<0.05$, §§$P<0.01$ vs 3E+VEGF (n=8 to 10). Data represent means±SEM. D, Ischemic limbs of wild-type mice (WT) and Sema3E-deficient mice (Sema3E KO) were analyzed for blood flow recovery (left) and vessel area (right). Sema3E-deficient mice showed better blood flow recovery and a larger vessel area of ischemic limbs. *$P<0.05$ vs WT mice (n=3 to 8). Data represent means±SEM.

Inhibition of Sema3E Improves Angiogenesis in Diabetic Mice

It has been reported that the angiogenic response to ischemia is attenuated in patients with diabetes.[19] We created a murine model of type 1 diabetes by intraperitoneal injection of streptozotocin (50 mg/kg per day for 5 days) and examined neovascularization after the animals were subjected to hind-limb ischemia. Blood glucose level was significantly higher and blood insulin level was significantly lower in streptozotocin-induced diabetic mice than in control mice (Online Figure V, A). Mice with streptozotocin-induced diabetes also showed poor blood flow recovery and a smaller vessel area in their ischemic limbs compared with control mice (Figure 5A and 5B). To investigate whether the impairment of neovascularization in diabetic mice was related to p53 and Sema3E, we examined the expression of these proteins in the mice. Western blot analysis revealed that p53 expression was increased in diabetic mice and that this increase was further enhanced by ischemia (Figure 5C; Online Figure V, B; and data not shown). Likewise, expression of Sema3E was significantly increased in diabetic mice compared with control mice (Figure 5C; Online Figure V, B). Consequently, blood flow recovery and the increase of the vessel area after VEGF treatment were significantly impaired in diabetic mice compared with VEGF-treated control mice (Figure 5A and 5B). To further assess the effect of inhibition of Sema3E in diabetic mice, we injected an expression vector encoding the plexinD1-Fc gene into the ischemic limbs of diabetic mice. Laser Doppler perfusion imaging of ischemic limbs and immunohistochemistry for CD31 revealed that the poor response of neovascularization to VEGF treatment was effectively overcome by introduction of the plexinD1-Fc gene (Figure 5D), suggesting that overexpression of Sema3E was responsible for impairment of neovascularization in the diabetic mice. These results indicate that inhibition of Sema3E is effective for promoting angiogenesis, especially when VEGF treatment is ineffective, such as in the diabetic state.

Discussion

The present study demonstrated that the Sema3E/plexinD1 axis inhibits postnatal angiogenesis in a murine model of

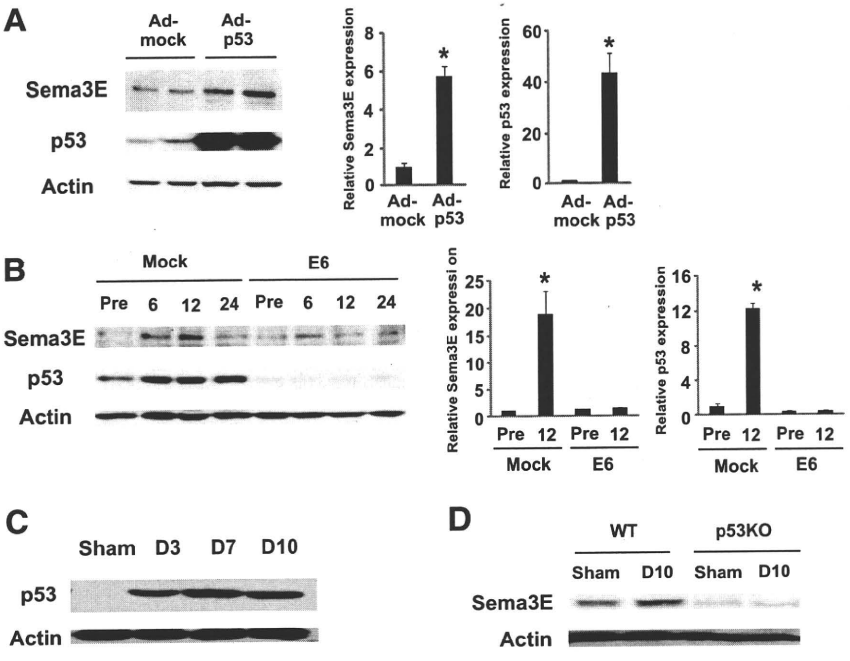

Figure 4. p53 regulates expression of Sema3E. A, Endothelial cells were infected with an adenoviral vector encoding p53 (Ad-p53) or mock (Ad-mock) and subjected to Western blot analysis for expression of Sema3E and p53 (left). Relative expression levels of Sema3E and p53 were plotted in the graph (right). *$P<0.01$ vs Ad-mock (n=4). Overexpression of p53 upregulated Sema3E expression. B, Endothelial cells were infected with a retroviral vector encoding HPV16 E6 (E6) or mock (Mock) and treated with $CoCl_2$ (100 μmol/L) for 6, 12, 24 hours (6, 12, 24). Expression of Sema3E and p53 was examined by Western blot analysis (left). Relative expression levels of Sema3E and p53 were plotted in the graph (right). *$P<0.05$ vs control (Pre) (n=3). Treatment with $CoCl_2$ markedly upregulated Sema3E expression compared to control (Pre), and this upregulation was inhibited by disruption of p53. C, Western blot analysis for p53 expression on day 3 (D3), day 7 (D7), and day 10 (D10) after surgery (n=4). Sham indicates sham-operated. Expression of p53 was markedly upregulated 3 days after surgery, and this upregulation persisted for 10 days. D, Western blot analysis for Sema3E expression in ischemic limbs of wild-type (WT) or p53-deficient (p53KO) mice on day 10 after surgery (n=4). Sema3E expression was increased in ischemic limbs of wild-type mice but not p53-deficient mice.

hindlimb ischemia. Our results also suggested that Sema3E inhibits angiogenesis by blocking activation of the VEGFR-2 and its downstream signaling pathway. Although Sema3E does not bind to neuropilin-1,[10] attraction of axons by Sema3E requires the presence of neuropilin-1 in addition to plexinD1, so the mode of assembly of the ligand and receptor complex is thought to determine the function of Sema3E.[20] Neuropilin-1 also binds to the VEGFR-2 and plays a crucial role in the regulation of VEGF signaling.[21] Accordingly, Sema3E may inhibit VEGF-induced angiogenesis by limiting the availability of neuropillin-1. Because treatment with an anti-VEGF neutralizing antibody did not completely over-

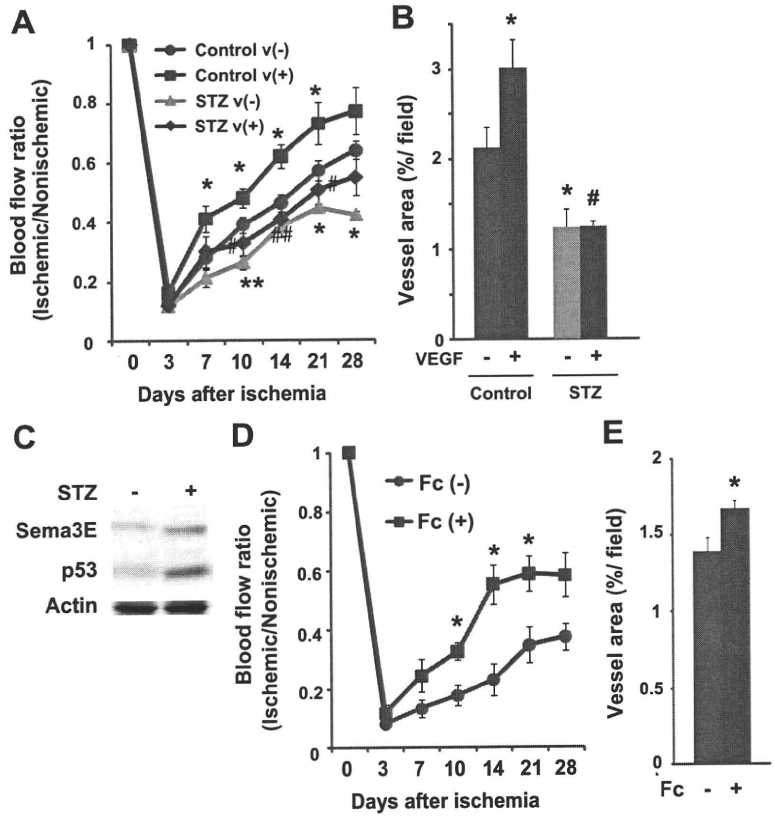

Figure 5. Sema3E inhibition improves impaired angiogenesis in diabetic mice. A and B, Blood flow recovery (A) and vessel area (B) in ischemic limbs of control (control) or streptozotocin-induced diabetic (STZ) mice after treatment with mock [v(−)] or the VEGF expression vector [v(+)]. Diabetic mice showed impaired blood recovery and a smaller vessel area in ischemic limbs compared with control mice. They showed less response to VEGF treatment. *$P<0.05$, **$P<0.01$ vs control/v(−); #$P<0.05$, ##$P<0.01$ vs control/v(+) (n=5 to 12). Data represent means±SEM. C, Expression of Sema3E and p53 was examined in limb tissues of control (STZ−) and streptozotocin-induced diabetic mice (STZ+) by Western blot analysis (n=4). Expression of Sema3E and p53 was upregulated in diabetic mice. D and E, Blood flow recovery (D) and vessel area (E) were analyzed in ischemic limbs of diabetic mice treated with VEGF [Fc(−)] or VEGF+plexinD1-Fc [Fc(+)]. Treatment of plxinD1-Fc in addition to VEGF significantly improved neovascularization in diabetic mice. *$P<0.01$ vs Fc(−) (n=7 to 9). Data represent means±SEM.

come the inhibitory effect of Sema3E on angiogenesis, this effect may also be attributable to the signaling pathway downstream of Sema3E-plexinD1, which is currently unknown.

Sema3E suppressed VEGF-induced phosphorylation of ERK and Akt (Figure 1D). It is well accepted that both ERK and Akt are crucial for the intracellular signaling pathways stimulated by hepatocyte growth factor (HGF) or basic fibroblast growth factor basic (bFGF) to induce angiogenesis. Interestingly, Sema3E also inhibited bFGF or HGF-induced tube formation in a dose-dependent manner (Online Figure VI, A). Moreover, Sema3E significantly inhibited bFGF-induced tube formation even in the presence of the anti-VEGF antibody, whereas it did not inhibit HGF-induced tube formation (Online Figure VI, B). These results suggest that besides the suppression of VEGF-induced angiogenesis, the antiangiogenic effect of Sema3E was partially mediated by VEGF-independent mechanisms.

It is known that intersomitic vessels are disorganized in Sema3E-deficient mice,[10] and this phenotype is markedly similar to that observed in mice lacking plexinD1.[13,14] However, whereas plexinD1-deficient mice develop severe cardiovascular defects involving the outflow tract of the heart and derivatives of the aortic arch arteries that result in perinatal death,[13] Sema3E-deficient mice do not show any large vessel abnormalities and do not undergo embryonic death. PlexinD1 has also been reported to bind to other semaphorins besides Sema3E, such as Sema3A,[13] Sema3C,[22] and Sema4A.[23] It has been shown that Sema3E only binds to plexinD1, whereas Sema3A and Sema3C bind to plexinA1 as well as to plexinD1.[5,10] Sema3A-deficient mice show neural path-finding defects and abnormalities of vascular development that result in neonatal death.[24–26] Ablation of the Sema3C gene in mice results in severe outflow tract abnormalities and mispatterning of intersomitic vessels.[27] Because plexinA1 deficiency also leads to cardiovascular defects,[28] Sema3A/C may play a pivotal role in embryonic vascular development regulated by the plexinA1/D1 pathway. More recently, Sema3A and Sema4A have been shown to inhibit postnatal angiogenesis,[29] suggesting that plexinD1-Fc treatment increases blood flow recovery in ischemic limbs by inhibiting Sema3E but also Sema3A/4A. Sema4D also has an inhibitory effect on postnatal angiogenesis[30]; however, it remains to be determined whether Sema4D binds to plexinD1.

Our results further suggest that p53 has a crucial role in the induction of Sema3E expression in ischemic tissue, although the precise mechanism of how p53 regulates Sema3E expression remains unknown. Because the antiangiogenic activity of p53 is important for tumor suppression, Sema3E/plexinD1 could be a potential target for the treatment of malignancies with p53 mutations. It has been reported that hyperglycemia activates p53 by increasing the production of reactive oxygen species.[31] Thus, p53-induced upregulation of antiangiogenic factors (including Sema3E) is likely to account for the impairment of angiogenesis in patients with diabetes. Therefore, Sema3E/plexinD1 could also be a target for the treatment of ischemic cardiovascular disease in diabetic patients because conventional therapeutic angiogenesis is not very efficient in this patient population.[32,33]

Acknowledgment

We thank Christopher Henderson, Columbia University, New York, for providing us with Sema3E knockout mice.

Sources of Funding

This work was supported by a Grant-in-Aid for Scientific Research from the Ministry of Education, Science, Sports, and Culture and Health and Labor Sciences Research Grants (to I.K.); a Grant-in-Aid for Scientific Research from the Ministry of Education, Culture, Sports, Science and Technology of Japan and grants from the Suzuken Memorial Foundation, the Japan Diabetes Foundation, the Ichiro Kanehara Foundation, the Tokyo Biochemical Research Foundation, the Takeda Science Foundation, the Cell Science Research Foundation, and the Japan Foundation of Applied Enzymology (to T.M.).

Disclosures

None.

References

1. Carmeliet P, Tessier-Lavigne M. Common mechanisms of nerve and blood vessel wiring. *Nature*. 2005;436:193–200.
2. Dickson BJ. Molecular mechanisms of axon guidance. *Science*. 2002; 298:1959–1964.
3. Weinstein BM. Vessels and nerves: marching to the same tune. *Cell*. 2005;120:299–302.
4. Eichmann A, Le Noble F, Autiero M, Carmeliet P. Guidance of vascular and neural network formation. *Curr Opin Neurobiol*. 2005;15:108–115.
5. Neufeld G, Kessler O. The semaphorins: versatile regulators of tumour progression and tumour angiogenesis. *Nat Rev Cancer*. 2008;8:632–645.
6. Luo Y, Raible D, Raper JA. Collapsin: a protein in brain that induces the collapse and paralysis of neuronal growth cones. *Cell*. 1993;75:217–227.
7. Tamagnone L, Artigiani S, Chen H, He Z, Ming GI, Song H, Chedotal A, Winberg ML, Goodman CS, Poo M, Tessier-Lavigne M, Comoglio PM. Plexins are a large family of receptors for transmembrane, secreted, and GPI-anchored semaphorins in vertebrates. *Cell*. 1999;99:71–80.
8. Ohta K, Mizutani A, Kawakami A, Murakami Y, Kasuya Y, Takagi S, Tanaka H, Fujisawa H. Plexin: a novel neuronal cell surface molecule that mediates cell adhesion via a homophilic binding mechanism in the presence of calcium ions. *Neuron*. 1995;14:1189–1199.
9. Song H, Ming G, He Z, Lehmann M, McKerracher L, Tessier-Lavigne M, Poo M. Conversion of neuronal growth cone responses from repulsion to attraction by cyclic nucleotides. *Science*. 1998;281:1515–1518.
10. Kruger RP, Aurandt J, Guan KL. Semaphorins command cells to move. *Nat Rev Mol Cell Biol*. 2005;6:789–800.
11. Roth L, Koncina E, Satkauskas S, Cremel G, Aunis D, Bagnard D. The many faces of semaphorins: from development to pathology. *Cell Mol Life Sci*. 2009;66:649–666.
12. Christensen CR, Klingelhofer J, Tarabykina S, Hulgaard EF, Kramerov D, Lukanidin E. Transcription of a novel mouse semaphorin gene, M-semaH, correlates with the metastatic ability of mouse tumor cell lines. *Cancer Res*. 1998;58:1238–1244.
13. Gitler AD, Lu MM, Epstein JA. PlexinD1 and semaphorin signaling are required in endothelial cells for cardiovascular development. *Dev Cell*. 2004;7:107–116.
14. Torres-Vazquez J, Gitler AD, Fraser SD, Berk JD, Van NP, Fishman MC, Childs S, Epstein JA, Weinstein BM. Semaphorin-plexin signaling guides patterning of the developing vasculature. *Dev Cell*. 2004;7:117–123.
15. Minamino T, Mitsialis SA, Kourembanas S. Hypoxia extends the life span of vascular smooth muscle cells through telomerase activation. *Mol Cell Biol*. 2001;21:3336–3342.
16. Couffinhal T, Silver M, Zheng LP, Kearney M, Witzenbichler B, Isner JM. Mouse model of angiogenesis. *Am J Pathol*. 1998;152:1667–1679.
17. Harris SL, Levine AJ. The p53 pathway: positive and negative feedback loops. *Oncogene*. 2005;24:2899–2908.
18. Teodoro JG, Parker AE, Zhu X, Green MR. p53-mediated inhibition of angiogenesis through up-regulation of a collagen prolyl hydroxylase. *Science*. 2006;313:968–971.

19. Falanga V. Wound healing and its impairment in the diabetic foot. *Lancet.* 2005;366:1736–1743.
20. Chauvet S, Cohen S, Yoshida Y, Fekrane L, Livet J, Gayet O, Segu L, Buhot MC, Jessell TM, Henderson CE, Mann F. Gating of Sema3E/PlexinD1 signaling by neuropilin-1 switches axonal repulsion to attraction during brain development. *Neuron.* 2007;56:807–822.
21. Soker S, Takashima S, Miao HQ, Neufeld G, Klagsbrun M. Neuropilin-1 is expressed by endothelial and tumor cells as an isoform-specific receptor for vascular endothelial growth factor. *Cell.* 1998;92:735–745.
22. Banu N, Teichman J, Dunlap-Brown M, Villegas G, Tufro A. Semaphorin 3C regulates endothelial cell function by increasing integrin activity. *FASEB J.* 2006;20:2150–2152.
23. Toyofuku T, Yabuki M, Kamei J, Kamei M, Makino N, Kumanogoh A, Hori M. Semaphorin-4A, an activator for T-cell-mediated immunity, suppresses angiogenesis via Plexin-D1. *EMBO J.* 2007;26:1373–1384.
24. Behar O, Golden JA, Mashimo H, Schoen FJ, Fishman MC. Semaphorin III is needed for normal patterning and growth of nerves, bones and heart. *Nature.* 1996;383:525–528.
25. Taniguchi M, Yuasa S, Fujisawa H, Naruse I, Saga S, Mishina M, Yagi T. Disruption of semaphorin III/D gene causes severe abnormality in peripheral nerve projection. *Neuron.* 1997;19:519–530.
26. Serini G, Valdembri D, Zanivan S, Morterra G, Burkhardt C, Caccavari F, Zammataro L, Primo L, Tamagnone L, Logan M, Tessier-Lavigne M, Taniguchi M, Puschel AW, Bussolino F. Class 3 semaphorins control vascular morphogenesis by inhibiting integrin function. *Nature.* 2003;424:391–397.
27. Feiner L, Webber AL, Brown CB, Lu MM, Jia L, Feinstein P, Mombaerts P, Epstein JA, Raper JA. Targeted disruption of semaphorin 3C leads to persistent truncus arteriosus and aortic arch interruption. *Development.* 2001;128:3061–3070.
28. Toyofuku T, Zhang H, Kumanogoh A, Takegahara N, Suto F, Kamei J, Aoki K, Yabuki M, Hori M, Fujisawa H, Kikutani H. Dual roles of Sema6D in cardiac morphogenesis through region-specific association of its receptor, Plexin-A1, with off-track and vascular endothelial growth factor receptor type 2. *Genes Dev.* 2004;18:435–447.
29. Maione F, Molla F, Meda C, Latini R, Zentilin L, Giacca M, Seano G, Serini G, Bussolino F, Giraudo E. Semaphorin 3A is an endogenous angiogenesis inhibitor that blocks tumor growth and normalizes tumor vasculature in transgenic mouse models. *J Clin Invest.* 2009;119:3356–3372.
30. Sun Q, Zhou H, Binmadi NO, Basile JR. Hypoxia inducible factor-1-mediated regulation of Semaphorin 4D affects tumor growth and vascularity. *J Biol Chem.* 2009;284:32066–32074.
31. Brodsky SV, Gealekman O, Chen J, Zhang F, Togashi N, Crabtree M, Gross SS, Nasjletti A, Goligorsky MS. Prevention and reversal of premature endothelial cell senescence and vasculopathy in obesity-induced diabetes by ebselen. *Circ Res.* 2004;94:377–384.
32. Losordo DW, Dimmeler S. Therapeutic angiogenesis and vasculogenesis for ischemic disease. Part I: angiogenic cytokines. *Circulation.* 2004;109:2487–2491.
33. Losordo DW, Dimmeler S. Therapeutic angiogenesis and vasculogenesis for ischemic disease. Part II: cell-based therapies. *Circulation.* 2004;109:2692–2697.

Excessive cardiac insulin signaling exacerbates systolic dysfunction induced by pressure overload in rodents

Ippei Shimizu,[1] Tohru Minamino,[1,2] Haruhiro Toko,[1] Sho Okada,[1] Hiroyuki Ikeda,[1] Noritaka Yasuda,[1] Kaoru Tateno,[1] Junji Moriya,[1] Masataka Yokoyama,[1] Aika Nojima,[1] Gou Young Koh,[3] Hiroshi Akazawa,[1] Ichiro Shiojima,[4] C. Ronald Kahn,[5] E. Dale Abel,[6] and Issei Komuro[1,4]

[1]Department of Cardiovascular Science and Medicine, Chiba University Graduate School of Medicine, Chiba, Japan. [2]PRESTO, Japan Science and Technology Agency, Saitama, Japan. [3]Biomedical Research Center and Biological Sciences, Korea Advanced Institute of Science and Technology, Daejeon, Korea. [4]Department of Cardiovascular Medicine, Osaka University School of Medicine, Osaka, Japan. [5]Joslin Diabetes Center, Harvard Medical School, Boston, Massachusetts, USA. [6]Division of Endocrinology, Metabolism and Diabetes and Program in Molecular Medicine, University of Utah School of Medicine, Salt Lake City, Utah, USA.

Although many animal studies indicate insulin has cardioprotective effects, clinical studies suggest a link between insulin resistance (hyperinsulinemia) and heart failure (HF). Here we have demonstrated that excessive cardiac insulin signaling exacerbates systolic dysfunction induced by pressure overload in rodents. Chronic pressure overload induced hepatic insulin resistance and plasma insulin level elevation. In contrast, cardiac insulin signaling was upregulated by chronic pressure overload because of mechanical stretch–induced activation of cardiomyocyte insulin receptors and upregulation of insulin receptor and Irs1 expression. Chronic pressure overload increased the mismatch between cardiomyocyte size and vascularity, thereby inducing myocardial hypoxia and cardiomyocyte death. Inhibition of hyperinsulinemia substantially improved pressure overload–induced cardiac dysfunction, improving myocardial hypoxia and decreasing cardiomyocyte death. Likewise, the cardiomyocyte-specific reduction of insulin receptor expression prevented cardiac ischemia and hypertrophy and attenuated systolic dysfunction due to pressure overload. Conversely, treatment of type 1 diabetic mice with insulin improved hyperglycemia during pressure overload, but increased myocardial ischemia and cardiomyocyte death, thereby inducing HF. Promoting angiogenesis restored the cardiac dysfunction induced by insulin treatment. We therefore suggest that the use of insulin to control hyperglycemia could be harmful in the setting of pressure overload and that modulation of insulin signaling is crucial for the treatment of HF.

Introduction

Cardiac hypertrophy is defined as an increment of ventricular mass resulting from increased cardiomyocyte size and is the adaptive response of the heart to an increased hemodynamic load due to either physiological factors such as exercise or pathological states such as hypertension and valvular diseases (1). Exercise-induced cardiac hypertrophy does not progress to heart failure (HF) (2, 3) and therefore is thought to be "physiological hypertrophy." On the other hand, pressure overload initially induces "adaptive hypertrophy," but causes "maladaptive (pathological) hypertrophy" in the chronic phase that results in HF (1).

Several signaling pathways have been implicated in the development of physiological or pathological cardiac hypertrophy. The insulin/PI3K/Akt axis plays a crucial role in the development of physiological hypertrophy as well as in normal cardiac growth, whereas activation of G-protein–coupled receptors in collaboration with PKC and calcineurin/nuclear factor of activated T cells (NFAT) pathways is involved in the development of pathological hypertrophy (4). Although homozygous cardiomyocyte-specific insulin receptor knockout (CIRKO) mice have smaller hearts than WT controls (5), both WT and CIRKO mice have shown a comparable increase of cardiac mass in response to pathological hypertrophic stimuli such as pressure overload (6). Overexpression of constitutively active p110α, a catalytic component of PI3K, in the heart has led to enhanced cardiac growth with preserved systolic function (7). Conversely, myocardial expression of dominant-negative p110α has inhibited the physiological hypertrophic response during postnatal growth and following exercise in mice, whereas the response to pressure overload has not been altered (8). Likewise, homozygous *Akt1*-deficient mice have shown defective exercise-induced cardiac hypertrophy (9), further supporting a crucial role of the insulin/PI3K/Akt pathway in physiological hypertrophy and growth of the heart.

Besides their role in physiological hypertrophy and normal cardiac growth, insulin signals may induce pathological hypertrophic responses. It has been shown that chronic hyperinsulinemia stimulates angiotensin II signaling that is involved in pathological hypertrophy (10). Mild to moderate activation of Akt was shown to induce cardiac hypertrophy with preservation of function (11, 12), whereas high levels of activated Akt expression in the heart led to pathological hypertrophy (13). Short-term Akt activation induced physiological cardiac hypertrophy, but constitutive activation of this pathway led to cardiac dysfunction (14). In this state, coordinated tissue growth and angiogenesis in the heart were disrupted, leading to myocardial hypoxia (14). Likewise, it has been demonstrated that chronic pressure overload increases the mismatch between cardiomyocyte size and vascularity and therefore induces

Authorship note: Ippei Shimizu and Tohru Minamino contributed equally to this work.

Conflict of interest: The authors have declared that no conflict of interest exists.

Citation for this article: *J Clin Invest.* 2010;120(5):1506–1514. doi:10.1172/JCI40096.

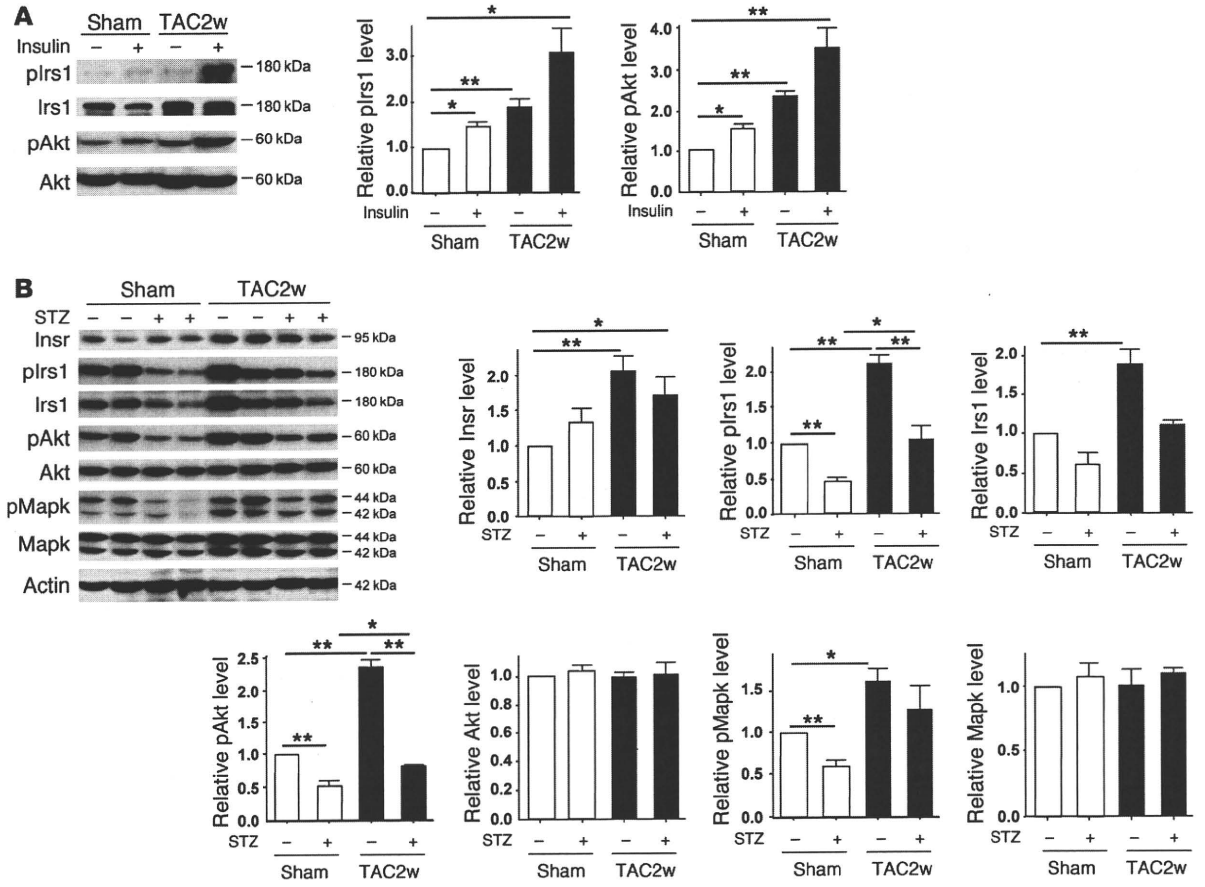

Figure 1

Upregulation of cardiac insulin signals by pressure overload. (**A**) Mice were subjected to TAC or sham operation (sham), and heart samples were obtained 2 weeks later. Mice were starved for 6 hours, and insulin or PBS was injected before sacrifice. pIrs1 and pAkt levels in the heart were examined by Western blot analysis. The graphs indicate relative expression levels of pIrs1 and pAkt. $n = 3$. TAC2w, 2 weeks after TAC. (**B**) Mice were subjected to TAC or sham operation and were sacrificed 2 weeks later. Components of the insulin signaling pathway in the heart were examined by Western blot analysis. The graphs indicate relative expression levels of these signaling molecules. $n = 3$. Data are shown as mean ± SEM. $^*P < 0.05$; $^{**}P < 0.01$.

myocardial hypoxia and cardiomyocyte death, leading to cardiac dysfunction (15). Moreover, intensive glycemic control of diabetic patients by insulin treatment has been reported to increase cardiovascular events (16). In the present study, we examined the role of insulin signaling in the development of cardiac dysfunction induced by pressure overload.

Results

Cardiac insulin signaling is activated by pressure overload. To investigate the role of the insulin signal pathway in failing hearts, we created severe transverse aortic constriction (TAC) in mice at 11 weeks of age. In this model, cardiac hypertrophy gradually progressed and reached a peak on day 7 after TAC (Supplemental Figure 1; supplemental material available online with this article; doi:10.1172/JCI40096DS1). Systolic function was preserved until day 7 but was significantly decreased on day 14 along with left ventricular dilatation (Supplemental Figure 1). Seven and fourteen days after TAC, we treated the mice with insulin (1 IU/kg) before sacrifice and examined the downstream signaling pathway of the insulin receptor (Insr) in the heart. Insulin-induced phosphorylation of insulin receptor substrate-1 (pIrs1) and Akt (pAkt) was markedly upregulated in the hearts of the TAC group compared with the sham-operated group (Figure 1A and Supplemental Figure 2A). We also found that the insulin signal pathway was constitutively activated in the TAC hearts under fasting conditions (Figure 1B and Supplemental Figure 2B). Expression of Insr and Irs1 protein as well as pIrs1 and pAkt protein was significantly increased in the TAC heart. These results suggest that chronic pressure overload upregulates cardiac insulin signaling. Enhanced insulin signaling was also observed in the hearts of spontaneously hypertensive rats (Supplemental Figure 3A).

Reduction of plasma insulin ameliorates systolic dysfunction induced by pressure overload. To determine whether upregulation of cardiac insulin signals has a pathological role in HF, we treated the mice with streptozotocin (STZ) (50 mg/kg i.p. for 5 days) at 4 weeks before TAC. Injection of STZ markedly decreased plasma insulin to below detectable levels, while the plasma glucose level gradually increased (Supplemental Figure 4). Pressure overload led to prominent cardiac hypertrophy along with upregulation of cardiac insulin signaling (Figure 1B and Figure 2, A and B). Systolic function was impaired and the left ventricular systolic dimension

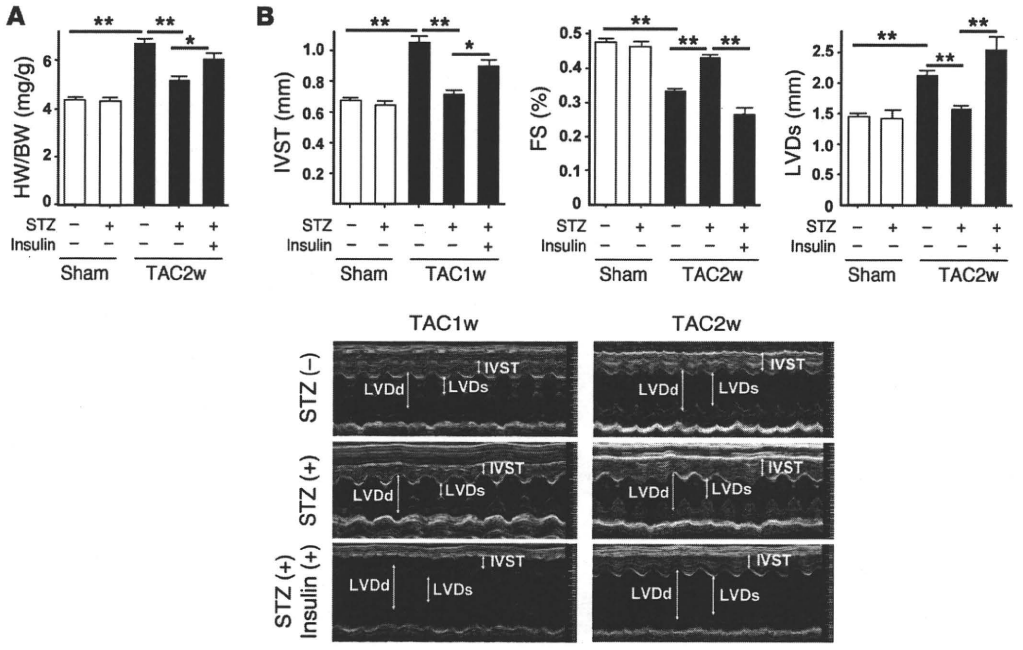

Figure 2

Depletion of plasma insulin attenuates systolic dysfunction induced by pressure overload. (**A**) STZ- or vehicle-treated mice were subjected to TAC or sham operation. The heart weight/body weight (HW/BW) ratio was measured 2 weeks after operation. In the insulin-treated group, daily i.p. injection of insulin (0.1 IU/g/d) was performed from 9 weeks (2 weeks after STZ treatment) to 13 weeks of age (2 weeks after TAC). n = 22–24. (**B**) Cardiac hypertrophy and systolic function of the animals prepared for **A** were estimated by echocardiography at 1 week (IVST) or 2 weeks (FS and LVDs) after operation. Photographs show representative results of echocardiography (M-mode). n = 6–10. Data are shown as mean ± SEM. $^*P < 0.05$; $^{**}P < 0.01$. IVST, intraventricular septal thickness; FS, fractional shortening.

(LVDs) was increased at 14 days after TAC (Figure 2, A and B). These alterations were significantly ameliorated in the mice treated with STZ (Figure 1B and Figure 2, A and B). Similar results were obtained at 6 weeks after TAC (Supplemental Figure 2C). We next examined the effect of insulin on cardiac function in this setting. STZ-treated mice were subjected to daily injection of insulin (0.1 IU/g/d from 9 weeks to 13 weeks of age) and to TAC at 11 weeks of age. Insulin treatment significantly improved hyperglycemia (Supplemental Figure 4). However, this treatment significantly enhanced cardiac hypertrophy and decreased systolic function along with left ventricular dilatation (Figure 2, A and B), indicating that insulin signaling influenced the development of systolic dysfunction due to pressure overload.

Reduction of plasma insulin inhibits cardiac hypoxia during pressure overload. We have recently demonstrated that cardiac angiogenesis is critically involved in the adaptive mechanism of cardiac hypertrophy and that an increased mismatch between cardiomyocyte size and vascularity is a crucial determinant of the transition from cardiac hypertrophy to HF (15). Consistent with our previous results, chronic pressure overload increased the cross-sectional area (CSA) of cardiomyocytes and decreased the relative vascularity (number of vessels/number of cardiomyocytes/CSA) (Figure 3, A–C), which in turn led to exacerbation of myocardial hypoxia (Figure 3D) and cardiomyocyte death (Figure 3E). In contrast, the increase of CSA after TAC was significantly attenuated by STZ treatment and the relative vascular density was markedly increased (Figure 3, A–C). Consequently, depletion of plasma insulin prevented cardiac hypoxia and cardiomyocyte death during chronic pressure overload (Figure 3, D and E). Conversely, insulin treatment of STZ-treated mice increased CSA and decreased relative vascular density, thereby exacerbating cardiac hypoxia and cardiomyocyte death (Figure 3, A–E). Additional treatment with the proangiogenic factor cartilage oligomeric matrix protein–angiopoietin-1 (COMP-Ang1) (17) increased relative vascular density and thereby improved cardiac hypoxia and systolic dysfunction (Supplemental Figure 5, A–C). We also found that a decrease of relative vascular density was associated with cardiac dysfunction, along with upregulation of insulin signaling in spontaneously hypertensive rats (Supplemental Figure 3, A–G), suggesting that cardiac insulin signaling plays a pathological role in HF by increasing a mismatch between cardiomyocyte size and vascularity.

Cardiomyocyte-specific reduction of Insr expression attenuates systolic dysfunction due to pressure overload. To further investigate the role of cardiac insulin signaling, we generated CIRKO mice by using the Cre-loxP system. We prepared transgenic mice in which a transgene encoding Cre recombinase was driven by the cardiomyocyte-specific α–myosin heavy chain (MHC) promoter (18). We then crossed these MHC-Cre mice with mice bearing floxed *Insr* alleles (19) and produced TAC in the resulting mice. Since homozygous CIRKO ($Insr^{flox/flox}Cre^+$) mice have been shown to develop systolic dysfunction in response to pressure overload (6), we utilized heterozygous CIRKO ($Insr^{flox/+}Cre^+$) mice with reduced cardiac expression of Insr (Figure 4A). These mice had a normal heart size and normal systolic function under physiological conditions (Figure 4, B and C). However, cardiac insulin signaling was markedly attenuated in the TAC heart of CIRKO mice (Figure 4B), and therefore chronic pressure

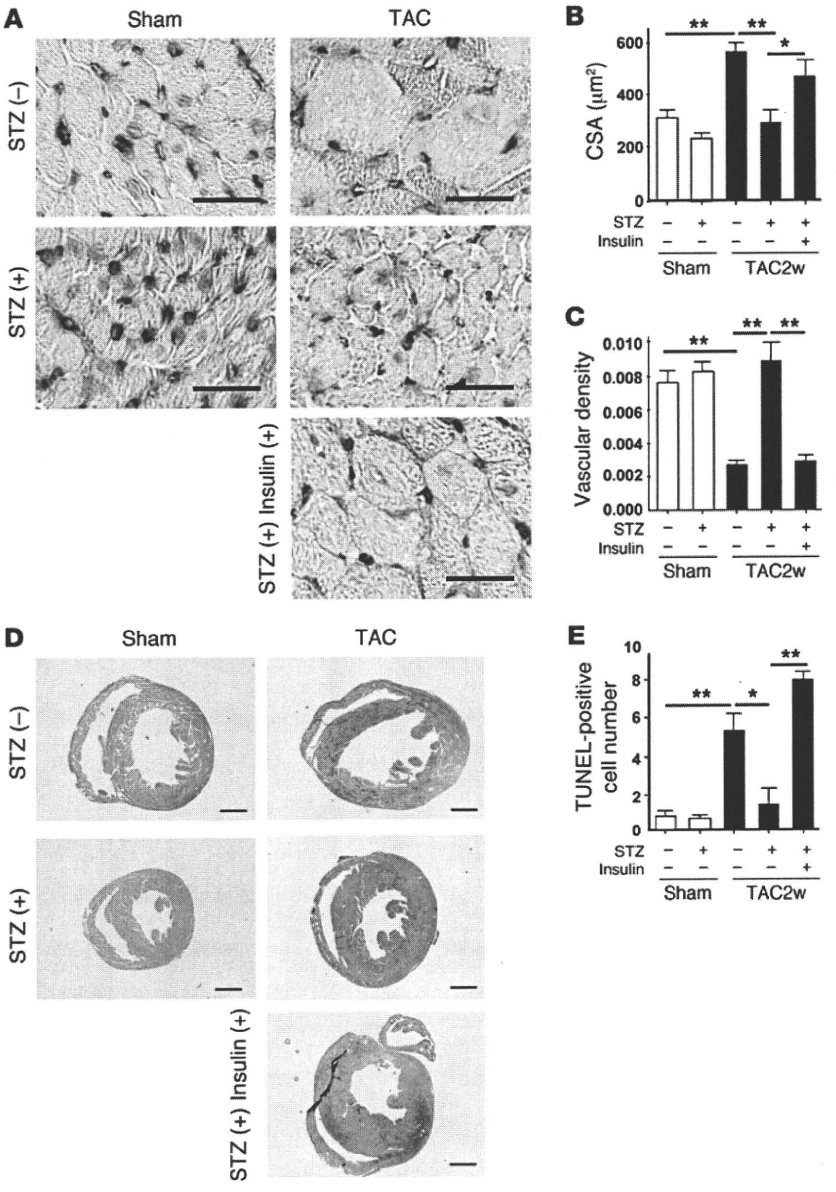

Figure 3

Reduction of plasma insulin inhibits cardiac hypoxia due to pressure overload. (**A**) Animals were prepared as described for Figure 2A. Immunohistochemistry using antibodies against platelet and endothelial cell adhesion molecule (dark brown) and dystrophin (light brown) was performed at 2 weeks after operation. Scale bars: 20 μm. (**B** and **C**) CSA of cardiomyocytes (**B**) and relative vascular density (**C**) were estimated as described in Methods. $n = 4–5$. (**D**) Cardiac ischemia (brown) in mice prepared as described for Figure 2A was estimated with a Hypoxyprobe-1. Scale bars: 1 mm. (**E**) Number of TUNEL-positive cells per 1×10^4 cardiomyocytes. $n = 4–6$. Data are shown as mean ± SEM. $^*P < 0.05$; $^{**}P < 0.01$.

overload caused less severe hypertrophy than in WT mice (Figure 4, C and D). Both systolic dysfunction and left ventricular dilatation were significantly inhibited in CIRKO mice compared with their littermate controls (Figure 4D and Supplemental Figure 6). Histological examination showed that the increase of CSA after TAC was significantly attenuated and relative vascular density was markedly increased in CIRKO mice (Figure 5, A–C). In consequence, the number of dead cardiomyocytes was significantly smaller in CIRKO mice than in their littermate controls (Figure 5D).

To investigate the role of Akt in HF induced by pressure overload, we utilized heterozygous *Akt1*-deficient (*Akt1*$^{+/-}$) mice. Two weeks after TAC operation, both systolic dysfunction and left ventricular dilatation were significantly inhibited in *Akt1*$^{+/-}$ mice compared with their littermate controls (Figure 6A). Histological examination showed that the increase of CSA after TAC was significantly attenuated and relative vascular density was markedly increased in *Akt1*$^{+/-}$ mice (Figure 6, B and C), which was associated with decreased activation of Akt (Figure 6D). These data suggest that sustained activation of Akt could cause cardiac dysfunction under chronic pressure overload.

Mechanism of enhanced cardiac insulin signaling due to pressure overload. To investigate the additional mechanisms by which chronic pressure overload enhances insulin signaling in the heart, we examined pIrs1 levels immediately after TAC. Western blot analysis revealed that pressure overload markedly increased the pIrs1 level from as early as 1 minute after the operation (Figure 7A). Such activation was significantly attenuated in both heterozygous and homozygous CIRKO mice (Figure 7A and Supplemental Figure 7), suggesting that mechanical stress may also upregulate the insulin signaling pathway via direct activation of Insr independent of its ligand. To further investigate the influence of mechanical stress on insulin signaling, we stretched cultured cardiomyocytes by 20% and examined the changes in the pIrs1 level. Consistent with our hypothesis, stretching of cardiomyocytes led to marked activation of insulin sig-

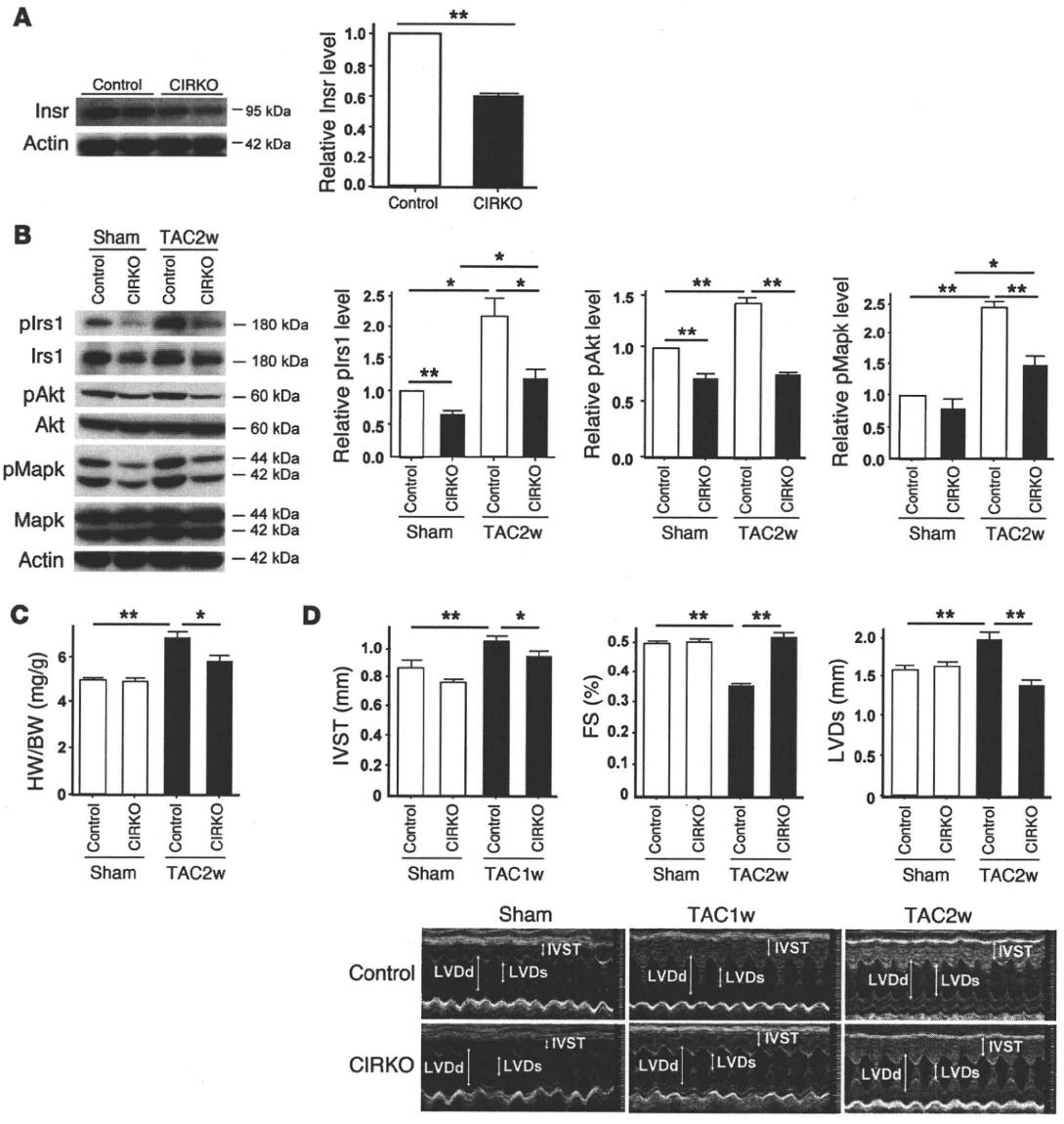

Figure 4

Cardiomyocyte-specific reduction of Insr expression attenuates systolic dysfunction due to pressure overload. (**A**) Western blot analysis of Insr expression in the hearts of CIRKO mice (*Insr*$^{flox/+}$Cre^{+}) and their littermate controls (control). Graphs indicate relative expression levels of Insr. $n = 3$. (**B**) CIRKO mice (*Insr*$^{flox/+}$Cre^{+}) or littermate controls were subjected to TAC or sham operation, and components of the insulin signaling pathway in the heart were examined by Western blot analysis at 2 weeks after operation. Graphs indicate relative expression levels of these signaling molecules. $n = 3$. (**C**) The heart weight/body weight ratio of animals prepared as described in **A** was measured at 2 weeks after operation. $n = 7–9$. (**D**) Cardiac hypertrophy and systolic function of animals prepared as described in **A** were assessed by echocardiography at 1 week (IVST) or 2 weeks (FS and LVDs) after operation. Photographs show representative results of echocardiography (M-mode). $n = 8–13$. Data are shown as mean ± SEM. $^{*}P < 0.05$; $^{**}P < 0.01$.

naling (Figure 7B). This activation was abolished by knockdown of Insr expression (Figure 7C), whereas knockdown of Igf1 or the Igf1 receptor showed a marginal effect (Supplemental Figure 8). These results suggest that mechanical stress mainly enhances insulin signaling through Insr and that Igf1 and the Igf1 receptor contribute to stretch-induced activation of this signaling to a lesser extent. This is similar to the known direct activation of the angiotensin II type I receptor by mechanical stress, which contributes to pathological hypertrophy (20); however, the precise mechanism of how mechanical stress activates insulin signaling needs further investigation.

There is accumulating evidence that suggests a potential relationship between insulin resistance and cardiac hypertrophy (21, 22). Therefore we examined plasma glucose and insulin levels in mice subjected to chronic pressure overload. Both glucose and insulin levels were significantly higher in the TAC group than in the sham-operated group (Figure 7D). More importantly, the homeostasis model assessment–insulin resistance (HOMA-IR) index was markedly elevated in the TAC group (Figure 7D). Furthermore, insulin-induced phosphorylation of Akt was impaired in the liver of the TAC group compared with the sham-operated group (Figure 7E).

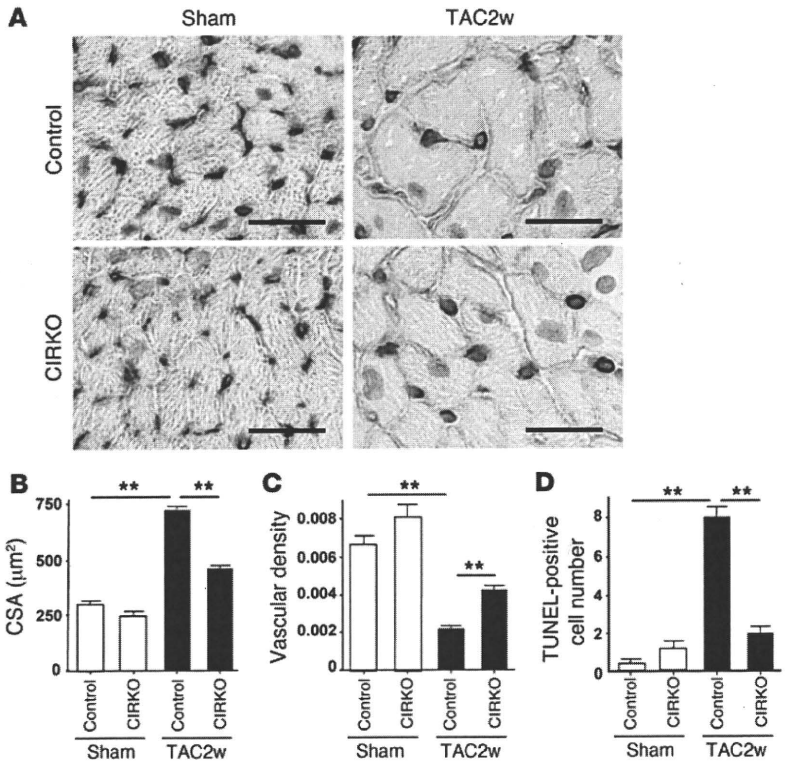

Figure 5
Cardiomyocyte-specific reduction of Insr expression attenuates cardiac hypoxia due to pressure overload. (**A**) CIRKO mice (*Insr*$^{flox/+}$Cre^{+}) or littermate controls were subjected to TAC or sham operation. Immunohistochemistry using antibodies against platelet and endothelial cell adhesion molecules (dark brown) and dystrophin (light brown) was performed at 2 weeks after operation. Scale bars: 20 μm. (**B** and **C**) CSA of cardiomyocytes (**B**) and relative vascular density (**C**) were estimated as described in Methods. $n = 4–5$. (**D**) Number of TUNEL-positive cells per 1×10^4 cardiomyocytes. $n = 4–5$. Data are shown as mean ± SEM. $^*P < 0.05$; $^{**}P < 0.01$.

These results suggest that chronic pressure overload induces hepatic insulin resistance, thereby inducing hyperinsulinemia, whereas there is no cardiac insulin resistance due to direct activation of Insr as well as to upregulation of Insr and Irs1.

Discussion

A number of clinical studies have strongly indicated the link between insulin resistance and nonischemic HF (23–26). Approximately two-thirds of patients with essential hypertension have abnormal glucose metabolism (27), and there is a positive relationship between cardiac hypertrophy and the plasma insulin concentration (28), suggesting that elevation of insulin contributes to myocardial growth in the presence of chronic pressure overload. Consistent with these reports, we found that chronic pressure overload induced hepatic insulin resistance and increased the plasma insulin level. Myocardial stretch activated Insr, and chronic pressure overload not only increased the activity of insulin signaling (pIrs1 and pAkt levels), but also upregulated the expression of Insr and Irs1 protein. This in turn facilitated activation of cardiac insulin signals by hyperinsulinemia. Such activation enhanced the mismatch between vascularity and cardiomyocyte size and increased cardiomyocyte death. This increase was associated with systolic dysfunction and may be one of the causes of HF induced by chronic pressure overload. However, we have not excluded other mechanisms by which excessive insulin signals promote cardiac dysfunction during pressure overload. For example, cardiac hypoxia may affect metabolism and contraction of myocytes with their viability being unchanged. Indeed, we only showed evidence for tissue hypoxia in the TAC heart by using pimonidazole, which may not be sufficient. We have not demonstrated that inhibition of cardiomyocyte death attenuates systolic dysfunction of the TAC heart. Accordingly, we cannot definitively conclude that hypoxia-induced cardiomyocyte death was essential for the development of HF. It has been reported that endothelial cells in the heart release a variety of factors, such as neuregulin and nitric oxide, that regulate survival and function of cardiomyocytes and that endothelial-myocardial interaction plays a crucial role in maintaining systolic function (29). Thus, it is also possible that a decrease of relative vascular density in the TAC heart impairs such paracrine mechanisms, leading to systolic dysfunction.

Our results were similar to those of the study with conditional Akt transgenic animals (14). In this model, Akt signaling could be switched on or off in the heart. These mice developed physiological hypertrophy following short-term induction, but exhibited pathological hypertrophy with longer periods of Akt activation due to an imbalance between cardiac growth and angiogenesis. Interestingly, cardiac dysfunction was further impaired when Akt was switched off after prolonged activation. These results suggest that Akt signaling itself is beneficial for maintenance of systolic function in this model; however, excessive cardiac growth with insufficient angiogenesis causes pathological hypertrophy. Thus, although insulin/Akt signaling has been implicated in the development of physiological hypertrophy, constitutive activation of these signals can induce HF when coordinated tissue growth and angiogenesis are disrupted.

Alterations of myocardial substrate metabolism have been implicated in the pathogenesis of contractile dysfunction and HF (21, 30). Studies on animal models of HF have demonstrated that, during transition from cardiac hypertrophy to ventricular dysfunction, expression of genes encoding for mitochondrial fatty acid (FA) β-oxidation enzymes shows a coordinated decrease, resulting in a shift of myocardial metabolism that recapitulates the fetal heart gene program, with glucose instead of FA becoming the primary energy substrate (31, 32). Clinical studies have revealed that patients with nonischemic cardiomyopathy exhibit alterations of

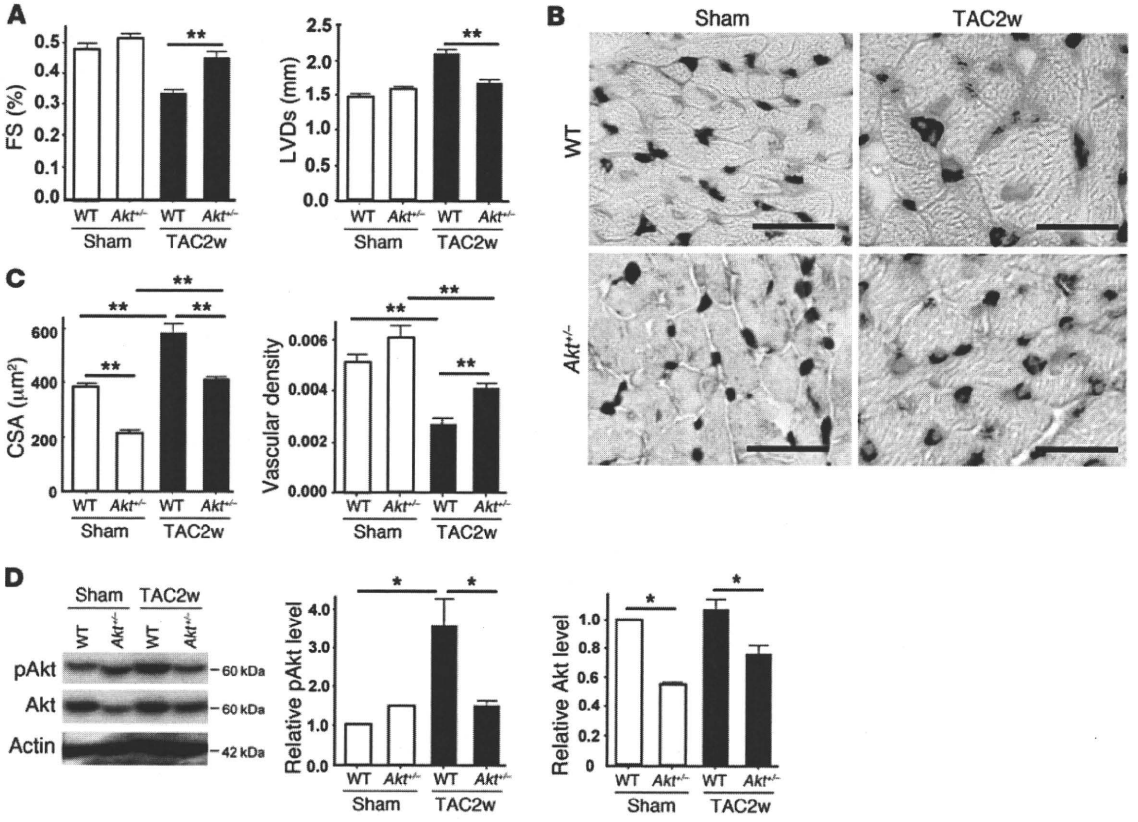

Figure 6

Reduced activation of Akt attenuates systolic dysfunction due to pressure overload. (**A**) *Akt1*-deficient (*Akt1*$^{+/-}$) mice and WT littermates were subjected to TAC or sham operation. Cardiac hypertrophy and systolic function were assessed by echocardiography at 2 weeks after operation. $n = 4$–6. (**B**) Immunohistochemistry using antibodies against platelet and endothelial cell adhesion molecules (dark brown) and dystrophin (light brown) was performed at 2 weeks after operation. Scale bars: 20 μm. (**C**) CSA of cardiomyocytes and relative vascular density were estimated as described in Methods. $n = 3$. (**D**) pAkt and Akt levels in the heart at 2 weeks after operation were examined by Western blot analysis. Graphs indicate relative expression levels of pAkt and Akt. $n = 3$. Data are shown as mean ± SEM. $^*P < 0.05$; $^{**}P < 0.01$.

myocardial metabolism that are characterized by a decrease of FA metabolism and an increase of myocardial glucose metabolism, a pattern similar to that shown in animal models of HF (33). Under these conditions, increased FA metabolism in the heart is pathogenic and the extent of abnormal FA metabolism predicts both morphologic changes of the heart and a poor clinical outcome (34). In this respect, activation of the insulin/Akt pathway in the failing heart appears to be an adaptive response, but constitutive activation of this pathway also leads to activation of growth signals that results in dysregulated hypertrophy, cardiac hypoxia, and systolic dysfunction. Thus, a metabolic modulator that increases glucose uptake (or decreases FA metabolism) without activation of insulin signaling would be a better strategy for the treatment of HF because these patients have systemic insulin resistance. Our results also suggest that the use of insulin to control hyperglycemia can be harmful, especially in the setting of pressure overload, a finding that is consistent with the outcome of a recent clinical trial (16).

Multiple counterregulatory hormones and cytokines are upregulated in HF and are likely to play a role in insulin resistance and altered glucose disposition (21). Upregulation of catecholamines not only contributes directly to the pathogenesis of cardiomyopathy but also increases insulin resistance and thereby indirectly affects systolic function. We also found that chronic pressure overload increased the production of proinflammatory cytokines by adipose tissue, thus promoting systemic insulin resistance (I. Shimizu and T. Minamino, unpublished observations). Further investigation of the link between insulin resistance and HF will continue to provide novel insights into the treatment of HF.

Methods

Animal models. All animal study protocols were approved by the Chiba University Review Board. C57BL/6 mice were purchased from SLC Japan. TAC was performed as described previously (15) in 11-week-old male mice. Sham-operated mice underwent the same procedure except for aortic constriction. For the type 1 diabetic model, 7-week-old male C57BL/6 mice were treated with i.p. STZ in 0.1 M sodium citrate (pH 4.5) at a dose of 50 mg/kg for 5 days. TAC was performed 4 weeks after STZ treatment. In the insulin-treated group, mice received daily i.p. injection of insulin (0.1 IU/g/d) from 9 weeks (2 weeks after STZ treatment) to 13 weeks of age (2 weeks after TAC). In some experiments, mice received an i.p. injection of insulin (1 IU/kg) 30 minutes before sacrifice to investigate the insulin sensitivity of various organs. *Akt1*-deficient mice (*Akt1*$^{+/-}$) were a gift from Morris J. Birnbaum (University of Pennsylvania School of Medicine, Philadelphia, Pennsylvania, USA). The generation and genotyping of *Akt1*-deficient mice, floxed *Insr* mice, and MHC-Cre mice have been described previously (18, 19, 35). Littermate controls have the genotype *Insr*$^{flox/+}$ or *Insr*$^{flox/flox}$. We

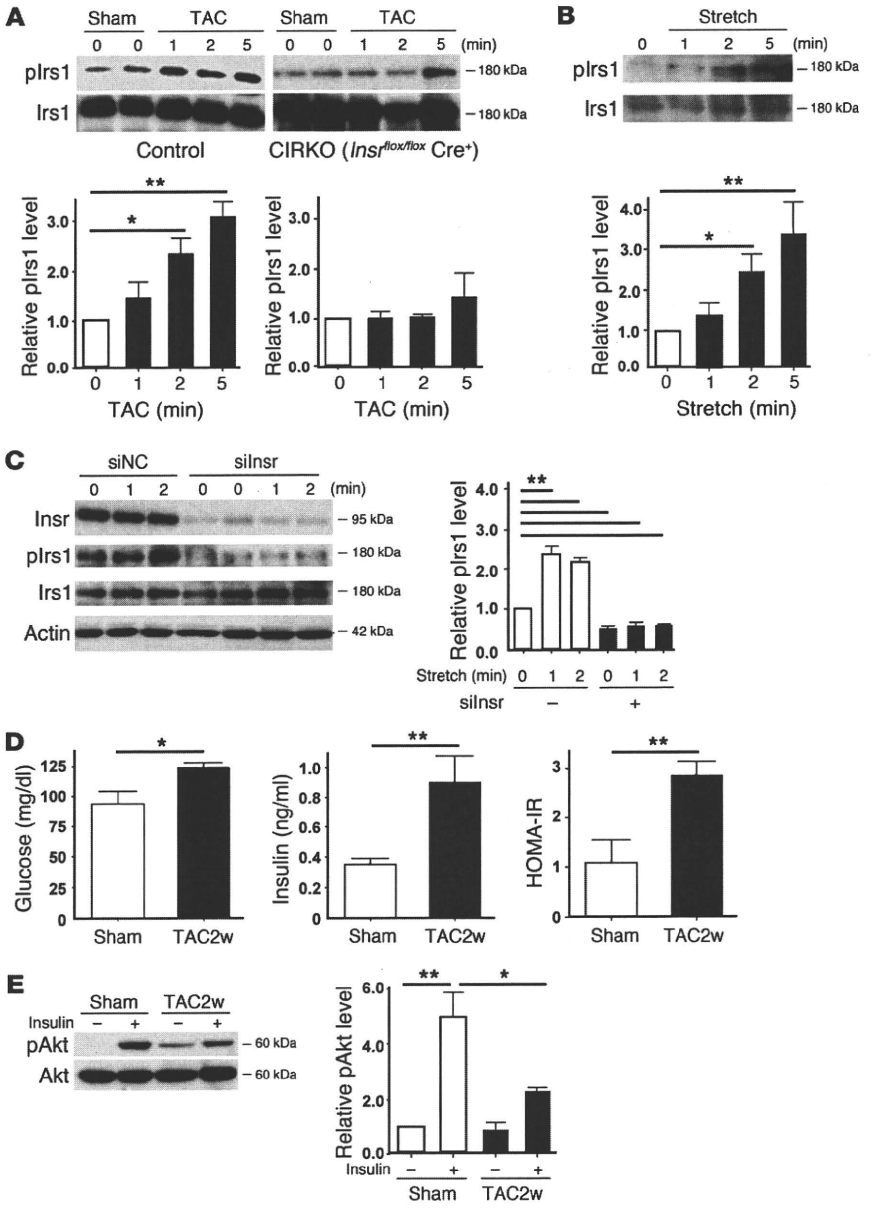

Figure 7

Mechanism of enhanced insulin signaling in the heart during pressure overload. (**A**) CIRKO mice (*Insr*$^{flox/flox}$Cre^{+}) or littermate controls were subjected to TAC or sham operation, and heart samples were obtained at the indicated times. pIrs1 levels were examined by Western blot analysis. The graphs indicate relative expression levels of pIrs1. $n = 3$. (**B**) Cardiomyocytes were subjected to mechanical stretch and pIrs1 levels were examined by Western blot analysis. $n = 3$. (**C**) siRNA targeting Insr (siInsr) or negative control RNA (siNC) was introduced into cardiomyocytes, after which the cells were subjected to mechanical stretch. pIrs1 levels were examined by Western blot analysis. $n = 3$. (**D**) Plasma glucose and insulin levels were examined at 2 weeks after TAC. $n = 7$–8. (**E**) Insulin-induced phosphorylation of Akt (pAkt) in the liver was examined after TAC or sham operation. $n = 3$. Data are shown as mean ± SEM. $^{*}P < 0.05$; $^{**}P < 0.01$.

administered adenoviral vector encoding COMP-Ang1 to mice i.v. after TAC operation as previously described (17).

Physiological and histological analyses. Echocardiography was performed with a Vevo 770 High Resolution Imaging System (Visual Sonics Inc.). To minimize variation of the data, the heart rate was always approximately 500–600 beats per minute when cardiac function was assessed. Cardiac tissue was fixed by perfusion with 4% paraformaldehyde. The fixed sample was immersed in OCT compounds (Miles Inc.) and snap-frozen in liquid nitrogen to prepare cryostat sections. Frozen cross sections of hearts were immunohistochemically double stained with antibodies for PECAM (BD Biosciences – Pharmingen) and dystrophin (Novocastra Laboratories). For measurement of the CSA of cardiomyocytes, 50 randomly selected cardiomyocytes in a left ventricular cross section were measured by tracing dystrophin immunostaining with NIH ImageJ software (http://rsbweb.nih.gov/ij/). Using the same sections, the number of PECAM-positive vessels was counted, and vascular density was estimated as the number of microvessels/number of cardiomyocytes/CSA. Tissue hypoxia was estimated with the Hypoxyprobe-1 (Chemicon) according to the manufacturer's instructions. Briefly, an i.p. injection of pimonidazole (60 mg/kg) was performed 90 minutes before sacrifice. Heart samples were harvested and fixed in 10% formalin overnight. The samples were embedded in paraffin, sectioned at 4-μm thickness, and stained with the Hypoxyprobe-1 monoclonal antibody (clone 4.3.11.3), which binds to protein adducts of pimonidazole in hypoxic cells. TUNEL labeling was performed according to the manufacturer's protocol (In Situ Apoptosis Detection Kit; TaKaRa) in combination with immunostaining for appropriate cell markers.

Western blot analysis. Whole-cell lysates were prepared in lysis buffer (10 mM Tris-HCl, pH 8, 140 mM NaCl, 5 mM EDTA, 0.025% NaN3, 1% Triton X-100, 1% deoxycholate, 0.1% SDS, 1 mM PMSF, 5 μg/ml leupeptin, 2 μg/ml aprotinin, 50 mM NaF, and 1 mM Na_2VO_3). The lysates (40–50 μg) were resolved by SDS-PAGE. Proteins were transferred to a PVDF membrane (Millipore), which was incubated with the primary antibody followed by anti-rabbit or anti-mouse immunoglobulin-G conjugated with horseradish peroxidase (Jackson). Specific proteins were detected by enhanced chemiluminescence

(Amersham). The primary antibodies used for Western blotting were as follows: anti-pIrs1 antibody (Tyr612, Biomol), anti-Irs1 antibody (C20), anti-Akt1 antibody (C20), anti-Insr β antibody (C-19) (Santa Cruz Biotechnology Inc.), anti-phospho-Akt antibody (Ser473), anti-phospho-p44/42 MAP kinase antibody (Thr202/Tyr204), anti-MAP kinase (ERK1+ERK2) antibody (Invitrogen), and anti-actin antibody (Sigma-Aldrich). Plasma insulin levels were evaluated with an ELISA kit (Morinaga Institute of Biological Science Inc.) according to the manufacturer's instructions.

Cell culture. Neonatal Wistar rats were purchased from Takasugi Experimental Animal Supply. Cardiomyocytes were prepared from neonatal rats and cultured as described previously (15). Passive stretching of cultured cells was done as described previously. Cells were plated on collagen-coated silicone rubber dishes (STREX Mechanical Cell Strain Instruments), and the silicone dishes were stretched by attaching both ends of each dish firmly to a fixed frame, resulting in longitudinal stretch by 20% of the original length. siRNA targeting Insr, IGF, and the IGF-1 receptor was purchased from Invitrogen and introduced into rat cardiomyocytes by using Lipofectamine RNAiMax (Invitrogen) according to the manufacturer's instructions.

Statistics. Data are shown as the mean ± SEM. Differences between groups were examined by 2-tailed Student's *t* test or ANOVA, followed by Bonferroni's correction for comparison of means. For all analyses, $P < 0.05$ was considered statistically significant.

Acknowledgments

We thank Morris J. Birnbaum for *Akt1*-deficient mice. This work was supported by a Grant-in-Aid for Scientific Research from the Ministry of Education, Science, Sports, and Culture and Health and Labor Sciences research grants (to I. Komuro); a Grant-in-Aid for Scientific Research from the Ministry of Education, Culture, Sports, Science and Technology of Japan; and grants from the Suzuken Memorial Foundation; the Japan Diabetes Foundation; the Ichiro Kanehara Foundation; the Tokyo Biochemical Research Foundation; the Takeda Science Foundation; the Cell Science Research Foundation; the Japan Foundation of Applied Enzymology; and the Astellas Foundation for Research on Metabolic Disorders (to T. Minamino).

Received for publication June 5, 2009, and accepted in revised form February 10, 2010.

Address correspondence to: Issei Komuro, Department of Cardiovascular Science and Medicine, Chiba University Graduate School of Medicine, 1-8-1 Inohana, Chuo-ku, Chiba 260-8670, Japan. Phone: 81.43.226.2097; Fax: 81.43.226.2557; E-mail: komuro-tky@umin.ac.jp.

1. Frey N, Olson EN. Cardiac hypertrophy: the good, the bad, and the ugly. *Annu Rev Physiol.* 2003;65:45–79.
2. Adams TD, Yanowitz FG, Fisher AG, Ridges JD, Lovell K, Pryor TA. Noninvasive evaluation of exercise training in college-age men. *Circulation.* 1981; 64(5):958–965.
3. Pelliccia A, Maron BJ. Outer limits of the athlete's heart, the effect of gender, and relevance to the differential diagnosis with primary cardiac diseases. *Cardiol Clin.* 1997;15(3):381–396.
4. Heineke J, Molkentin JD. Regulation of cardiac hypertrophy by intracellular signalling pathways. *Nat Rev Mol Cell Biol.* 2006;7(8):589–600.
5. Belke DD, et al. Insulin signaling coordinately regulates cardiac size, metabolism, and contractile protein isoform expression. *J Clin Invest.* 2002; 109(5):629–639.
6. Hu P, Zhang D, Swenson L, Chakrabarti G, Abel ED, Litwin SE. Minimally invasive aortic banding in mice: effects of altered cardiomyocyte insulin signaling during pressure overload. *Am J Physiol Heart Circ Physiol.* 2003;285(3):H1261–H1269.
7. Shioi T, et al. The conserved phosphoinositide 3-kinase pathway determines heart size in mice. *EMBO J.* 2000;19(11):2537–2548.
8. McMullen JR, et al. Phosphoinositide 3-kinase (p110α) plays a critical role for the induction of physiological, but not pathological, cardiac hypertrophy. *Proc Natl Acad Sci U S A.* 2003;100(21):12355–12360.
9. DeBosch B, et al. Akt1 is required for physiological cardiac growth. *Circulation.* 2006;113(17):2097–2104.
10. Samuelsson AM, et al. Hyperinsulinemia: effect on cardiac mass/function, angiotensin II receptor expression, and insulin signaling pathways. *Am J Physiol Heart Circ Physiol.* 2006;291(2):H787–H796.
11. Condorelli G, et al. Akt induces enhanced myocardial contractility and cell size in vivo in transgenic mice. *Proc Natl Acad Sci U S A.* 2002;99(19):12333–12338.
12. Matsui T, et al. Phenotypic spectrum caused by transgenic overexpression of activated Akt in the heart. *J Biol Chem.* 2002;277(25):22896–22901.
13. Shioi T, et al. Akt/protein kinase B promotes organ growth in transgenic mice. *Mol Cell Biol.* 2002; 22(8):2799–2809.
14. Shiojima I, et al. Disruption of coordinated cardiac hypertrophy and angiogenesis contributes to the transition to heart failure. *J Clin Invest.* 2005; 115(8):2108–2118.
15. Sano M, et al. p53-induced inhibition of Hif-1 causes cardiac dysfunction during pressure overload. *Nature.* 2007;446(7134):444–448.
16. Gerstein HC, et al. Effects of intensive glucose lowering in type 2 diabetes. *N Engl J Med.* 2008; 358(24):2545–2559.
17. Cho CH, et al. Long-term and sustained COMP-Ang1 induces long-lasting vascular enlargement and enhanced blood flow. *Circ Res.* 2005;97(1):86–94.
18. Abel ED, et al. Cardiac hypertrophy with preserved contractile function after selective deletion of GLUT4 from the heart. *J Clin Invest.* 1999;104(12):1703–1714.
19. Bruning JC, et al. A muscle-specific insulin receptor knockout exhibits features of the metabolic syndrome of NIDDM without altering glucose tolerance. *Mol Cell.* 1998;2(5):559–569.
20. Zou Y, et al. Mechanical stress activates angiotensin II type 1 receptor without the involvement of angiotensin II. *Nat Cell Biol.* 2004;6(6):499–506.
21. Witteles RM, Fowler MB. Insulin-resistant cardiomyopathy clinical evidence, mechanisms, and treatment options. *J Am Coll Cardiol.* 2008;51(2):93–102.
22. Sharma N, Okere IC, Duda MK, Chess DJ, O'Shea KM, Stanley WC. Potential impact of carbohydrate and fat intake on pathological left ventricular hypertrophy. *Cardiovasc Res.* 2007;73(2):257–268.
23. Swan JW, et al. Insulin resistance in chronic heart failure: relation to severity and etiology of heart failure. *J Am Coll Cardiol.* 1997;30(2):527–532.
24. Ingelsson E, Sundstrom J, Arnlov J, Zethelius B, Lind L. Insulin resistance and risk of congestive heart failure. *JAMA.* 2005;294(3):334–341.
25. Arnlov J, et al. Several factors associated with the insulin resistance syndrome are predictors of left ventricular systolic dysfunction in a male population after 20 years of follow-up. *Am Heart J.* 2001; 142(4):720–724.
26. Hasegawa S, Kusuoka H, Maruyama K, Nishimura T, Hori M, Hatazawa J. Myocardial positron emission computed tomographic images obtained with fluorine-18 fluoro-2-deoxyglucose predict the response of idiopathic dilated cardiomyopathy patients to beta-blockers. *J Am Coll Cardiol.* 2004; 43(2):224–233.
27. Garcia-Puig J, Ruilope LM, Luque M, Fernandez J, Ortega R, Dal-Re R. Glucose metabolism in patients with essential hypertension. *Am J Med.* 2006; 119(4):318–326.
28. Karason K, Sjostrom L, Wallentin I, Peltonen M. Impact of blood pressure and insulin on the relationship between body fat and left ventricular structure. *Eur Heart J.* 2003;24(16):1500–1505.
29. Brutsaert DL. Cardiac endothelial-myocardial signaling: its role in cardiac growth, contractile performance, and rhythmicity. *Physiol Rev.* 2003;83(1):59–115.
30. Neubauer S. The failing heart--an engine out of fuel. *N Engl J Med.* 2007;356(11):1140–1151.
31. Christe ME, Rodgers RL. Altered glucose and fatty acid oxidation in hearts of the spontaneously hypertensive rat. *J Mol Cell Cardiol.* 1994;26(10):1371–1375.
32. Barger PM, Kelly DP. Fatty acid utilization in the hypertrophied and failing heart: molecular regulatory mechanisms. *Am J Med Sci.* 1999;318(1):36–42.
33. Davila-Roman VG, et al. Altered myocardial fatty acid and glucose metabolism in idiopathic dilated cardiomyopathy. *J Am Coll Cardiol.* 2002;40(2):271–277.
34. Yazaki Y, et al. Assessment of myocardial fatty acid metabolic abnormalities in patients with idiopathic dilated cardiomyopathy using 123I BMIPP SPECT: correlation with clinicopathological findings and clinical course. *Heart.* 1999;81(2):153–159.
35. Cho H, Thorvaldsen JL, Chu Q, Feng F, Birnbaum MJ. Akt1/PKBalpha is required for normal growth but dispensable for maintenance of glucose homeostasis in mice. *J Biol Chem.* 2001;276(42):38349–38352.

Promotion of CHIP-Mediated p53 Degradation Protects the Heart From Ischemic Injury

Atsuhiko T. Naito, Sho Okada, Tohru Minamino, Koji Iwanaga, Mei-Lan Liu, Tomokazu Sumida, Seitaro Nomura, Naruhiko Sahara, Tatsuya Mizoroki, Akihiko Takashima, Hiroshi Akazawa, Toshio Nagai, Ichiro Shiojima, Issei Komuro

Rationale: The number of patients with coronary heart disease, including myocardial infarction, is increasing and novel therapeutic strategy is awaited. Tumor suppressor protein p53 accumulates in the myocardium after myocardial infarction, causes apoptosis of cardiomyocytes, and plays an important role in the progression into heart failure.

Objectives: We investigated the molecular mechanisms of p53 accumulation in the heart after myocardial infarction and tested whether anti-p53 approach would be effective against myocardial infarction.

Methods and Results: Through expression screening, we found that CHIP (carboxyl terminus of Hsp70-interacting protein) is an endogenous p53 antagonist in the heart. CHIP suppressed p53 level by ubiquitinating and inducing proteasomal degradation. CHIP transcription was downregulated after hypoxic stress and restoration of CHIP protein level prevented p53 accumulation after hypoxic stress. CHIP overexpression in vivo prevented p53 accumulation and cardiomyocyte apoptosis after myocardial infarction. Promotion of CHIP function by heat shock protein (Hsp)90 inhibitor, 17-allylamino-17-demethoxy geldanamycin (17-AAG), also prevented p53 accumulation and cardiomyocyte apoptosis both in vitro and in vivo. CHIP-mediated p53 degradation was at least one of the cardioprotective effects of 17-AAG.

Conclusions: We found that downregulation of CHIP level by hypoxia was responsible for p53 accumulation in the heart after myocardial infarction. Decreasing the amount of p53 prevented myocardial apoptosis and ameliorated ventricular remodeling after myocardial infarction. We conclude that anti-p53 approach would be effective to treat myocardial infarction. (*Circ Res.* 2010;106:1692-1702.)

Key Words: myocardial infarction ■ CHIP ■ p53 ■ hypoxia

The number of patients with coronary heart disease has been increasing and cardiovascular diseases are the leading cause of deaths in the Western world. Despite the development of pharmacological and nonpharmacological interventions, 33% of the men and 43% of the women die within 5 years after myocardial infarction (MI).[1] Therefore, a novel therapeutic approach against coronary heart disease is awaited.

Apoptosis of cardiomyocytes is accompanied with acute coronary occlusion.[2] Because apoptotic loss of cardiomyocytes causes heart failure,[3] inhibition of apoptosis has been suggested as an additional therapeutic approach to coronary heart disease.[4] In mice, overexpression of antiapoptotic Bcl-2 protein or genetic deletion of proapoptotic Bax protein have been reported to prevent apoptosis and reduce infarct size,[5–8] implicating that antiapoptotic approach is effective for prevention of ventricular remodeling after myocardial infarction.

The tumor suppressor *p53* is an important transcription factor that regulates cell cycle progression, cellular senescence, and apoptosis. Under physiological condition, p53 protein level is maintained low, but is elevated when cells are stressed or damaged.[9] The mechanism for keeping p53 protein level low involves several E3 ubiquitin ligases such as MDM2,[10,11] COP1,[12] and Pirh2.[13] Importantly, the expression of these proteins were positively regulated by p53, suggesting the role for negative-feedback loop against p53 elevation.

Protein level of p53 is also kept low in the heart but it is elevated when cardiac cells are exposed to hypoxia.[14–16]

Original received December 4, 2009; revision received April 6, 2010; accepted April 12, 2010.

From the Department of Cardiovascular Science and Medicine (A.T.N., S.O., T. Minamino, K.I., M.-L.L., T.S., S.N., H.A., T.N., I.S., I.K.), Chiba University Graduate School of Medicine, Japan; Department of Cardiovascular Medicine (A.T.N., H.A., I.S., I.K.), Osaka University Graduate School of Medicine, Japan; PRESTO (T. Minamino), Japan Science and Technology Agency, Saitama, Japan; and Laboratory for Alzheimer's Disease (N.S., T. Mizoroki, A.T.). RIKEN Brain Science Institute, Saitama, Japan.

This manuscript was sent to Junichi Sadoshima, Consulting Editor, for review by expert referees, editorial decision, and final disposition.

Correspondence to Issei Komuro, MD, PhD, Department of Cardiovascular Science and Medicine, Chiba University Graduate School of Medicine, 1-8-1 Inohana, Chuo-ku, Chiba, Japan. E-mail komuro-tky@umin.ac.jp

Circulation Research **is available at http://circres.ahajournals.org** **DOI: 10.1161/CIRCRESAHA.109.214346**

We have recently reported that elevation of p53 causes the development of pressure overload-induced heart failure.[16] We have also observed the elevation of p53 protein levels after myocardial infarction and shown that *p53* gene deletion improved cardiac function after myocardial infarction,[16] suggesting that the inhibition of p53 might become a novel therapeutic strategy for ischemic heart diseases.

As an initial approach for the investigation of anti-p53 therapy, we searched for an endogenous p53 antagonist in the heart. Through expression screening, we found that CHIP (carboxyl terminus of Hsp70-interacting protein) is an endogenous p53 antagonist that keeps p53 level low in the heart. We also found that CHIP downregulation is involved in the mechanism of p53 accumulation in the heart after myocardial infarction. Facilitating CHIP-mediated p53 degradation prevented apoptosis of cardiomyocytes and ameliorated ventricular remodeling in the postinfarct heart. The present study revealed the mechanism of p53 accumulation in the heart after myocardial ischemia and suggested that anti-p53 approach would be effective to treat myocardial infarction.

Non-standard Abbreviations and Acronyms

17-AAG	17-allylamino-17-demethoxy geldanamycin
CHIP	carboxyl terminus of Hsp70-interacting protein
HIF	hypoxia-inducible factor
HRE	hypoxia-responsive element
Hsp	heat shock protein
HW/BW	heart weight/body weight
MI	myocardial infarction
PARP	poly(ADP-ribose)polymerase
siRNA	small interfering RNA

Methods

Expression Cloning

Expression cloning was performed as described previously[17] using PG13-Luc (kind gift from B. Vogelstein, Ludwig Center for Cancer Genetics and Therapeutics, Howard Hughes Medical Institute, and Sidney Kimmel Cancer Center, Johns Hopkins Medical Institutions, Baltimore, Md) as a reporter plasmid. Initially, cDNA expression library from human heart (Invitrogen) was separated into small pools that contain ≈100 clones each. cDNA clones that downregulate PG13 activity were isolated by sib-selection.

Cell Culture

COS7 and HEK293 cells are from ATCC and cultured in DMEM containing 10% FBS (Invitrogen). Neonatal rat cardiomyocytes were isolated from 1-day-old Wistar rats and cultured as described previously.[18] Cardiomyocytes were exposed to hypoxic stress by culturing under $CoCl_2$ or by culturing in hypoxic chamber (<1% O_2; Po_2, 18 to ≈20 mm Hg).

Animals

All protocols were approved by Chiba University review board. CHIP knockout mice and cardiac-specific inducible hypoxia-inducible factor (HIF)-1 knockout mice were described.[16,19,20] Heterozygous CHIP knockout mice were used in this study because homozygous knockout mice were perinatally lethal.[20] Cardiac-specific CHIP transgenic mice were generated by pronuclear injection of αMHC-HA-CHIP transgene construct. Coronary artery ligation was performed on 10-week old male mice as described previously.[21]

Statistical Analysis

Data are expressed as means±SE. The significance of differences among means was evaluated using analysis of variance (ANOVA), followed by Fisher's protected least significant difference test and Dunnett's test for multiple comparisons. Significant differences were defined as $P<0.05$.

Results

Identification of CHIP As a Novel p53 Antagonist From Heart cDNA Library

To elucidate novel p53 antagonists in the heart, we performed expression screening by expressing cDNA pools in COS7 cells together with a reporter plasmid, PG13-luciferase, which contains 13 copies of p53 binding site upstream of luciferase gene and responsive to wild-type p53 dependent transcription. From the screening of 500 cDNA pools, each containing around 100 individual cDNA clones obtained from human heart cDNA library, we found 5 pools that suppress the PG13 activity. Individual cDNA clone that downregulates the PG13 activity was identified by sib-selection. One of the molecules that was highly expressed in the heart (Figure I, A, in the Online Data Supplement, available at http://circres.ahajournals.org) was CHIP (also called STUB1 [Stip1 homology and U-box containing protein]), a chaperone-interacting protein with E3 ubiquitin ligase activity.[22] Transfection of CHIP suppressed endogenous and exogenous (by overexpression of p53) PG13 activity (Figure 1A) and decreased the protein levels of p53 (Figure 1B) in a plasmid dose-dependent manner in COS7 cells. Direct interaction between CHIP and p53 was confirmed both at the exogenous level in COS7 cells (Online Figure I, B) and at the endogenous level in cardiomyocytes (Online Figure I, C). Western blotting using anti-ubiquitin antibody after immunoprecipitation with p53 revealed that overexpression of CHIP increased poly-ubiquitinated p53 (which appears as a smear) (Online Figure I, D). The proteasomal inhibitor MG132 restored p53 protein level that was suppressed by CHIP (Online Figure I, E), indicating that CHIP directs p53 for proteasome-mediated degradation. When CHIP was knocked down in cardiomyocytes using small interfering (si)RNA, p53 expression was upregulated (Figure 1C), and p53 protein levels following CHIP knockdown were comparable to those induced by the knockdown of MDM2, a well known E3 ubiquitin ligase for p53 (Figure 1D). CHIP protein level was not changed by knockdown of MDM2 (Figure 1D). p53 protein levels were also markedly elevated in the heart of CHIP heterozygous mice (Figure 1E). These results suggest that CHIP induces degradation of wild-type p53 protein in cardiomyocytes, which is consistent with previous reports in other cells (H1299 cells and U2OS cells).[23,24] In addition, we revealed that CHIP is a crucial negative regulator that keeps p53 protein levels low in the heart under physiological conditions.

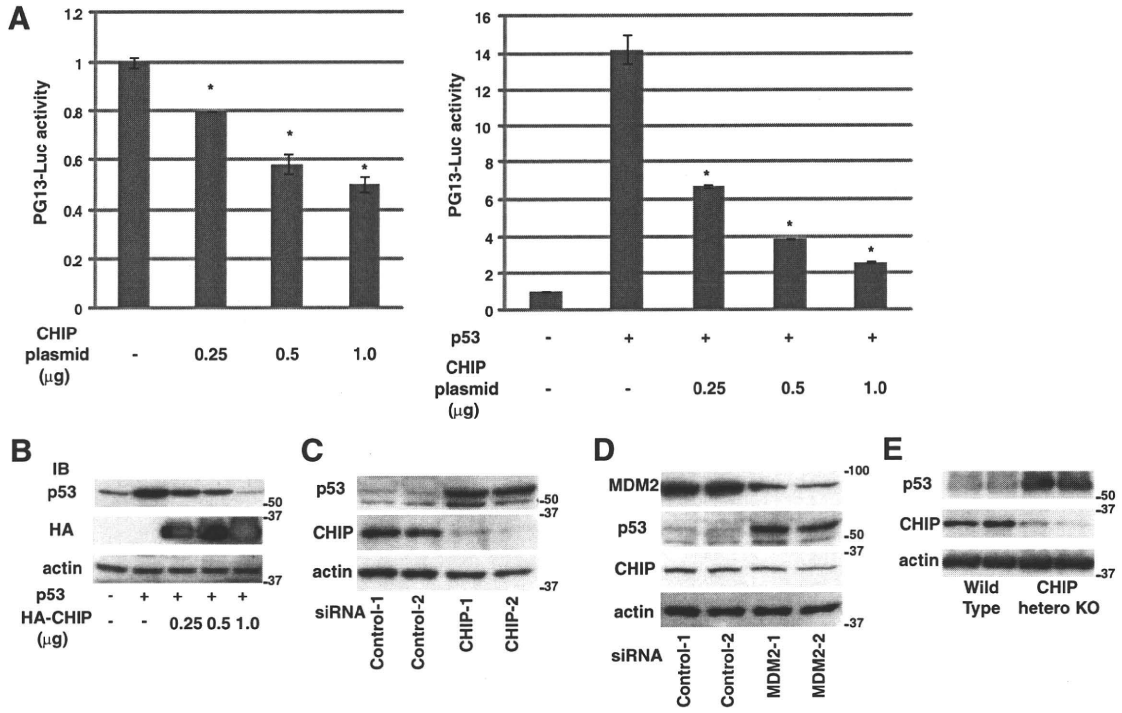

Figure 1. CHIP is a crucial negative regulator of p53 expression in the heart. A, Transfection of CHIP expressing plasmid suppressed endogenous **(left)** and exogenous **(right)** p53 transcriptional activity. *$P<0.01$ vs control; n=5. **B,** CHIP decreases p53 protein levels in COS7 cells. IB indicates immunoblot. **C,** p53 expression is upregulated by CHIP knockdown in cardiomyocytes. siRNAs specific to CHIP (CHIP-1 and CHIP-2), or control siRNA were transfected into cultured cardiomyocytes and protein levels of CHIP and p53 were examined by Western blotting. CHIP-1 and CHIP-2 represent 2 different siRNAs against CHIP. Control-1 is a commercially available control RNA, and control-2 is a scrambled control RNA. **D,** p53 upregulation is also observed by MDM2 knockdown. siRNAs specific to MDM2 (MDM2–1 and MDM2–2) or control siRNA were transfected into cultured cardiomyocytes, and protein levels of CHIP, p53, and MDM2 were examined by Western blotting. The extent of p53 upregulation by MDM2 knockdown was comparable to that induced by CHIP knockdown. **E,** Total protein of wild-type and CHIP heterozygous mice were analyzed by Western blotting. p53 expression is upregulated in the heart of CHIP heterozygous mice.

Molecular Mechanisms of Hypoxia-Induced p53 Accumulation

As CHIP regulates p53 status in the heart, we speculated that CHIP might be involved in the molecular mechanism of hypoxia-induced p53 accumulation in the heart. Cobalt chloride ($CoCl_2$) increases HIF-1 activity through preventing HIF-1α protein degradation and is widely used as a hypoxia mimicking reagent.[25,26] Treatment of cardiomyocytes with $CoCl_2$ (250 μmol/L) increased p53 protein level with a marked downregulation of CHIP protein level (Figure 2A). Notably, the expression of MDM2 was rather increased in this experimental condition. Because transcriptional regulation of MDM2 is known to be upregulated by p53 as a part of negative-feedback loop, increased MDM2 expression after $CoCl_2$ treatment may possibly be attributable to this feedback system against p53 elevation. Accumulation of p53 and downregulation of CHIP were also observed when cardiomyocytes were cultured in hypoxic chamber for 24 hours (Online Figure I, F). We confirmed that both treatments increased nuclear HIF-1α protein that binds to HIF-1α binding oligonucleotide by commercially available ELISA system (Online Figure I, G). We also analyzed the expression of p53 and CHIP in the heart after MI. p53 protein levels were increased on day 1 after MI and remained upregulated thereafter, whereas expression levels of CHIP were markedly downregulated on day 1, and remained at lower levels than those of controls (Figure 2B and analyzed in Online Figure II, A and B). In contrast, MDM2 protein levels were slightly increased after MI (Figure 2B). The inverse correlation between CHIP and p53 protein level implies the possible involvement of CHIP downregulation in the initiation of p53 accumulation after acute hypoxic stress. Other E3 ubiquitin ligases whose transcription is regulated by p53, such as MDM2, might work to reverse p53 level after initial accumulation of p53 as a feedback system to prevent further detrimental effects that might be elicited by chronic p53 elevation.

To investigate why CHIP is downregulated after hypoxic insult, we tested whether HIF-1 mediates hypoxia-induced downregulation of CHIP, because HIF-1 is known to downregulate some of its target genes through hypoxia-responsive element (HRE).[27–30] Human CHIP promoter (from −329 bases upstream of transcription start site to +39 bases downstream of transcription start site) that contains a conserved HRE at −49 (Figure 2C) was cloned upstream of luciferase reporter gene (pGL4-CHIP). pGL4-CHIP activity was significantly suppressed by both $CoCl_2$ treatment (24 hours) and HIF-1α overexpression in COS7 cells (Figure 2D). When a mutation was introduced into HRE at −49 (pGL4-CHIP-mutHRE), the luciferase activity was no longer responsive to hypoxic stress or HIF-1α overexpression (Figure 2D), suggesting that *CHIP* gene expression is downregu-

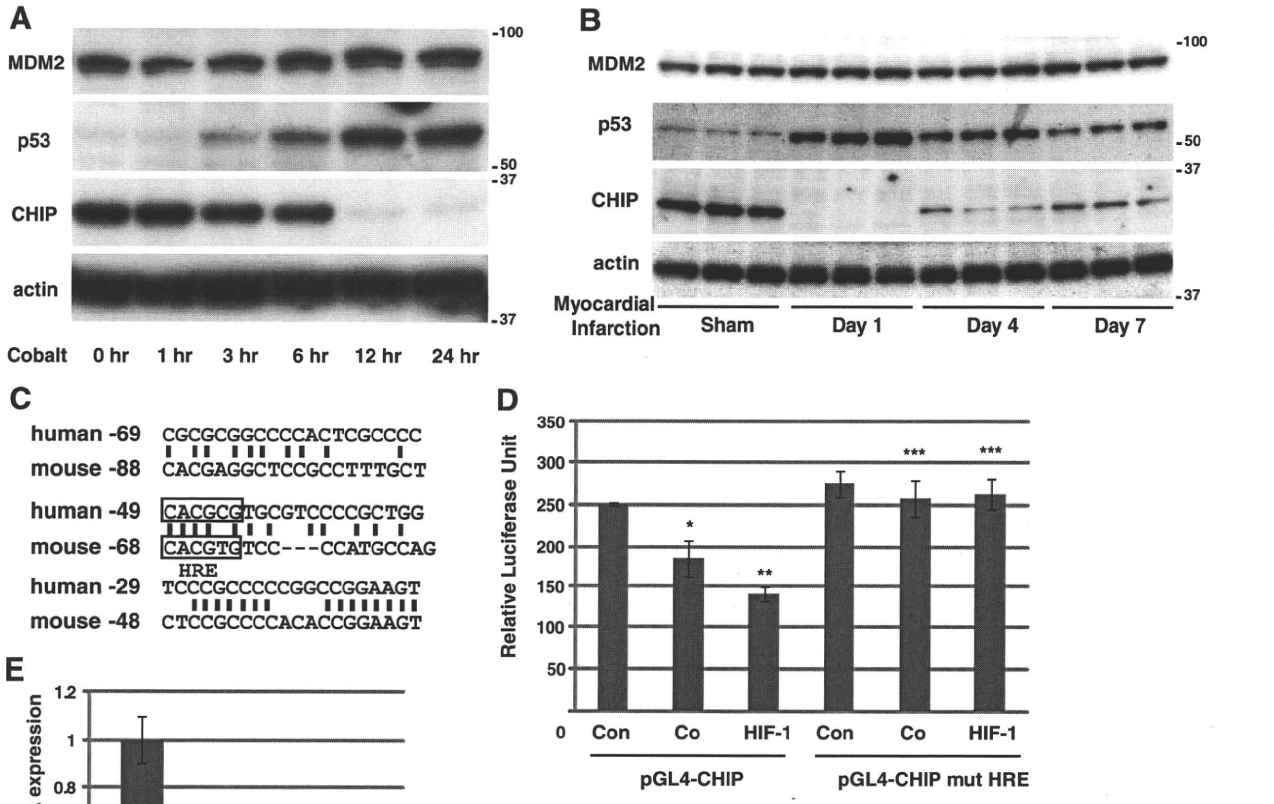

Figure 2. CHIP is downregulated by hypoxic stress. A, $CoCl_2$-induced p53 accumulation is associated with CHIP downregulation in cardiomyocytes. Cardiomyocytes were treated with 250 μmol/L $CoCl_2$, and protein was extracted at the indicated time point. **B,** Experimental myocardial infarction was created by permanent ligation of the coronary artery. Protein samples were extracted from total heart at the indicated time point after coronary artery ligation. CHIP expression is downregulated and p53 expression is upregulated after MI. **C,** Sequence comparison of human and mouse CHIP promoter. **Boxes** indicate conserved HRE. **D,** CHIP promoter activity is downregulated by $CoCl_2$ treatment and HIF-1α overexpression, and mutations (CACGTG to CTGGCG) introduced into HRE at −49 abrogated this response. CHIP promoter sequence from human genomic DNA (−329 to +39 from transcription start site) was cloned upstream of luciferase gene. Mutation was introduced using a kit from Stratagene. Luciferase assay was performed 24 hours after $CoCl_2$ treatment or HIF-1α overexpression. *P<0.05, **P<0.01, ***P=NS vs control; n=5. **E,** Real-time PCR analysis revealed mRNA level of CHIP was also downregulated by hypoxic stress (Co) and HIF-1α overexpression. RNA was extracted 24 hours after $CoCl_2$ treatment or HIF-1α overexpression. *P<0.01.

lated by HIF-1 at the transcriptional level through HRE. Real-time PCR analysis revealed that exposure of cardiomyocytes to $CoCl_2$ (24 hours) and adenoviral overexpression of constitutively active HIF-1α led to marked downregulation of CHIP mRNA levels (Figure 2E), further supporting our data that hypoxic stress downregulates CHIP levels. HIF-1α gene is both required and sufficient for hypoxic stress-induced CHIP downregulation and p53 accumulation because knockdown of HIF-1α attenuated the effects of $CoCl_2$ treatment on expressions of p53 and CHIP (Online Figure III, A), and overexpression of constitutively active HIF-1α suppressed CHIP expression and increased p53 expression in cardiomyocytes (Online Figure III, B). Furthermore, downregulation of CHIP protein levels after MI was attenuated in cardiac-specific inducible HIF-1α conditional knockout mice[16] (Online Figure III, C). Collectively, these findings suggest that CHIP transcription is directly downregulated by hypoxia through HIF-1.

CHIP Protects Cardiomyocytes From Hypoxia-Induced p53-Mediated Apoptosis of Cardiomyocytes

Because hypoxia or p53 overexpression induces apoptotic cell death in cultured cardiomyocytes,[14] we next examined whether hypoxia-induced cardiomyocyte apoptosis is mediated by the HIF-1-CHIP-p53 pathway. $CoCl_2$ treatment (24 hours) induced p53 accumulation and promoted apoptosis of cardiomyocytes as assessed by cleaved poly (ADP-ribose) polymerase (PARP) expression (Figure 3A), Annexin V staining (Figure 3B and 3C), and caspase-3 activity (Figure 3D). $CoCl_2$-induced apoptosis was p53-dependent, because knockdown of p53 in $CoCl_2$-treated cardiomyocytes attenuated hypoxia-induced cell death (Figure 3A through 3D). We next assessed whether overexpression of CHIP could rescue $CoCl_2$-induced apoptosis. Adenovirus-mediated overexpression of CHIP in cardiomyocytes markedly downregulated p53 expression and attenuated apoptosis in $CoCl_2$-treated

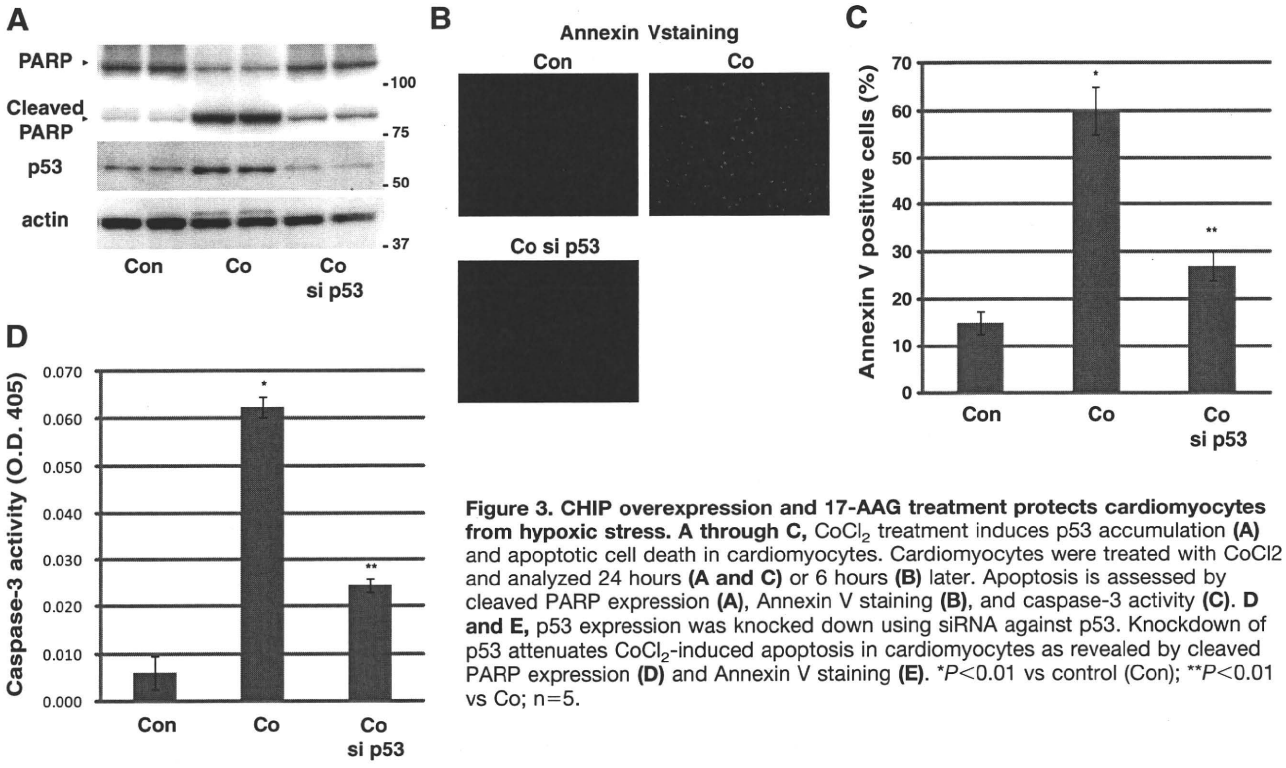

Figure 3. CHIP overexpression and 17-AAG treatment protects cardiomyocytes from hypoxic stress. A through C, $CoCl_2$ treatment induces p53 accumulation **(A)** and apoptotic cell death in cardiomyocytes. Cardiomyocytes were treated with CoCl2 and analyzed 24 hours **(A and C)** or 6 hours **(B)** later. Apoptosis is assessed by cleaved PARP expression **(A)**, Annexin V staining **(B)**, and caspase-3 activity **(C). D and E,** p53 expression was knocked down using siRNA against p53. Knockdown of p53 attenuates $CoCl_2$-induced apoptosis in cardiomyocytes as revealed by cleaved PARP expression **(D)** and Annexin V staining **(E).** $^*P<0.01$ vs control (Con); $^{**}P<0.01$ vs Co; n=5.

cardiomyocytes (Figure 4A through 4C). These results underscore our hypothesis that downregulation of CHIP is responsible for p53 accumulation after hypoxic stress. Moreover, forced expression of CHIP prevented hypoxia-induced cardiomyocyte apoptosis by inducing degradation of p53, suggesting that CHIP-mediated p53 degradation is a potential therapeutic target.

17-AAG Protects Cardiomyocytes From Hypoxia-Induced Apoptosis

Inhibitors for heat shock protein (Hsp)90 have been shown to promote proteasomal degradation of CHIP client proteins and to be effective for the diseases caused by the accumulation of CHIP substrates.[31,32] We therefore examined whether an Hsp90 inhibitor 17-allylamino-17-demethoxy geldanamycin (17-AAG) induces degradation of p53 protein and protects cardiomyocytes from hypoxic stress. In cardiomyocytes treated with $CoCl_2$, 17-AAG downregulated p53 expression (Figure 4D). 17-AAG treatment also suppressed hypoxia-induced cardiomyocyte apoptosis in a CHIP-dependent manner, because CHIP knockdown attenuated the protective effects of 17-AAG (Figure 4E through 4G). These results suggest that 17-AAG protects cardiomyocytes from hypoxic stress by promoting CHIP-mediated p53 degradation.

Interestingly, protein level of CHIP was increased by 17-AAG treatment (Figure 4E). As mRNA level of CHIP was not changed by 17-AAG treatment (Online Figure IV, A), we speculated that protein stability was affected by 17-AAG treatment. When protein translation was inhibited by cycloheximide, 17-AAG treatment dramatically extended the protein half-life of CHIP (Online Figure IV, B and C). 17-AAG also upregulated the protein stability of other proteins, Hsp70 and HSF-1 (Online Figure IV, B and C). Because 17-AAG exerted some antiapoptotic effects even in the cells of negligible CHIP protein level (Figure 4E and 4F), upregulation of these cardioprotective proteins[33,34] might mediate part of the effects of 17-AAG. It remains to be determined how 17-AAG prolongs protein half-life of certain kinds of proteins.

CHIP and 17-AAG Prevent Apoptosis and Ventricular Remodeling After Myocardial Infarction

We next examined whether promotion of CHIP-mediated p53 degradation could attenuate ischemic cardiac injury also in vivo. For this purpose, transgenic mice which overexpress CHIP specifically in the heart (CHIP-Tg) (Figure 5A) were subjected to permanent coronary artery ligation. In CHIP-Tg mice, elevation of p53 protein levels (Figure 5B) and apoptotic cardiomyocyte death in the border zone of the infarct area (Figure 5B and 5C) were attenuated compared to wild-type littermates at 24 hours after the MI operation. Apoptotic death of the cardiomyocytes in the remote zone of the infarct was not changed between littermates (data not shown). We next examined whether this decrease in apoptotic cell death leads to attenuation of cardiac ventricular remodeling. At day 14, CHIP-Tg mice exhibited smaller heart weight/body weight (HW/BW) ratio, better contractility and less ventricular remodeling (Figure 5D and 5E) compared to wild-type littermates. These results provides an evidence for our hypothesis that CHIP downregulation is responsible for p53 accumulation after myocardial infarction, and suggests that CHIP overexpression is protective for the heart by preventing p53 accumulation and cardiomyocyte apoptosis after myocardial infarction.

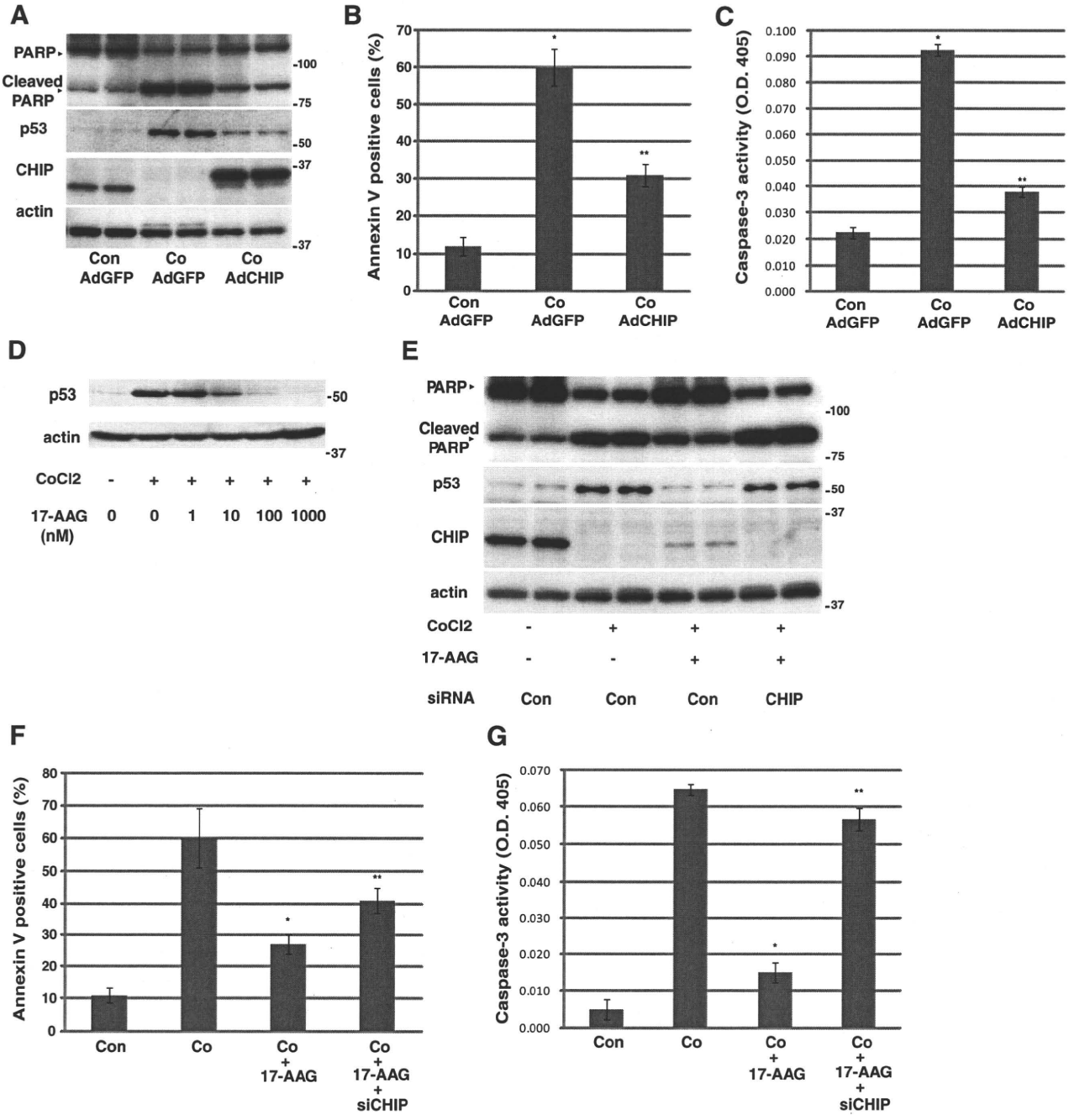

Figure 4. Promoting CHIP-mediated p53 degradation is protective against hypoxic stress. A through C, Overexpression of CHIP attenuates $CoCl_2$-induced p53 accumulation **(A)** and apoptosis in cardiomyocytes. Cardiomyocytes were infected with adenovirus harboring green fluorescent protein (GFP) or CHIP. Twenty-four hours later, culture medium was changed and the cells were treated with $CoCl_2$. Apoptosis was assessed by cleaved PARP expression **(A)**, Annexin V staining **(B)**, and caspase-3 activity **(C)**. *$P<0.01$ vs control (Con)+AdGFP; **$P<0.01$ vs Co+AdGFP; n=5. **D,** 17-AAG downregulates p53 expression in cardiomyocytes. Neonatal rat cardiomyocytes were treated with $CoCl_2$ with or without 17-AAG at the indicated concentration. **E through G,** 17-AAG inhibits $CoCl_2$-induced p53 accumulation **(E)** and apoptosis in cardiomyocytes, which is abrogated by CHIP knockdown. Neonatal rat cardiomyocytes were transfected with control siRNA or siRNA against CHIP. Twenty-four hours later, medium was changed and the cells were treated with $CoCl_2$ and/or 17-AAG. Apoptosis is assessed by cleaved PARP expression **(E)**, Annexin V staining **(F)**, and caspase-3 activity **(G)**. *$P<0.01$ vs Co; **$P<0.05$ vs Co +17-AAG; n=3.

We also examined whether treatment with 17-AAG exerts similar cardioprotective effects. 17-AAG (10 mg/kg) or vehicle was intraperitoneally injected immediately after permanent coronary artery ligation. This single injection of 17-AAG effectively suppressed the elevation of p53 protein levels and apoptotic cell death in the border zone of the infarct area at 24 hours after the operation (Figure 6A and 6B). As p53 protein level was kept elevated even 4 and 7 days after MI (Figure 2B), 17-AAG was injected every other days and we assessed whether 17-AAG treatment also leads to attenuation of ventricular remodeling, as observed in CHIP-Tg mice. At day 14, mice treated with 17-AAG exhibited smaller HW/BW ratio, better contractility,

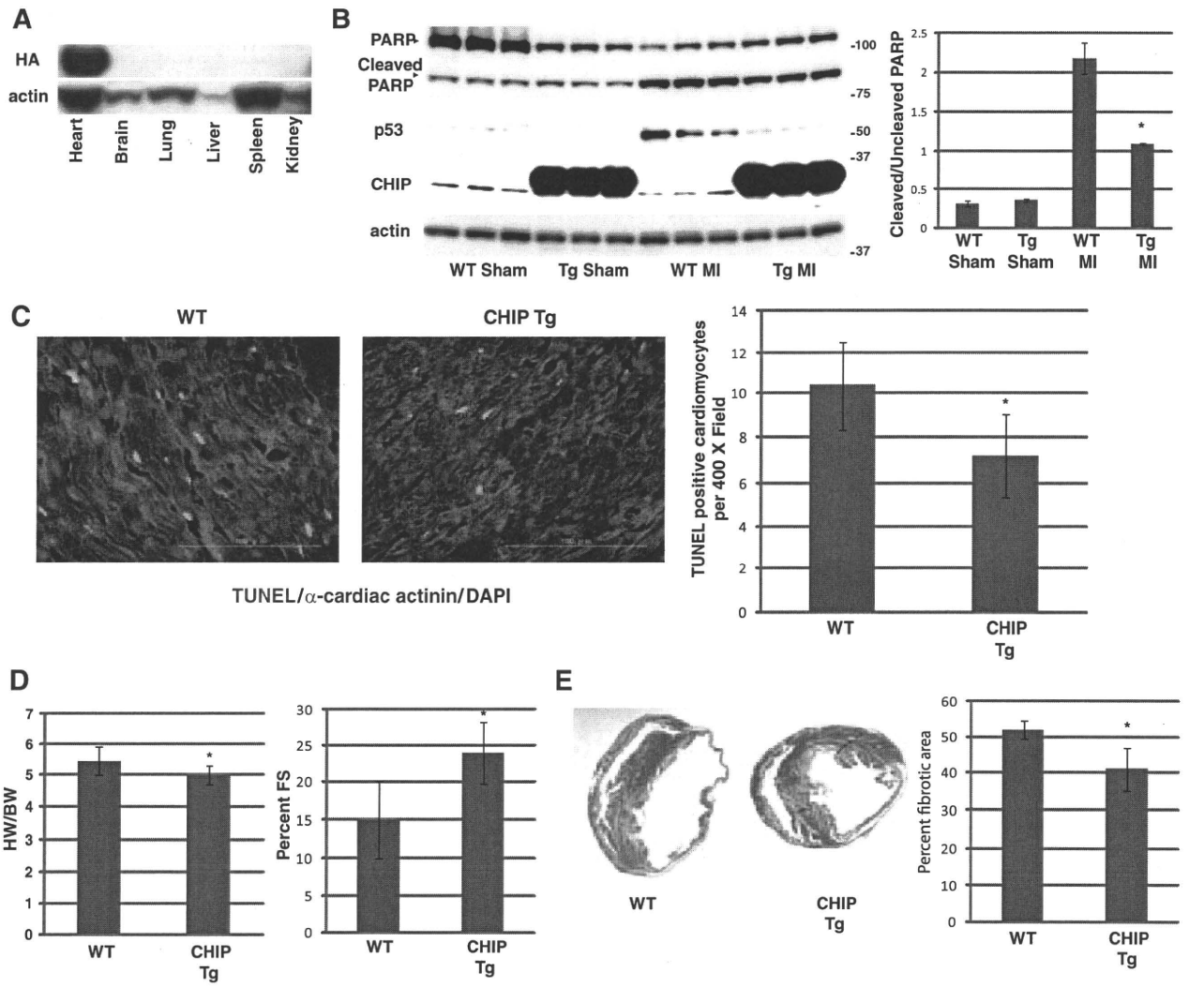

Figure 5. Overexpression of CHIP attenuates ischemic cardiac injury in vivo. A, Cardiac-specific expression of HA-tagged human CHIP in CHIP-Tg mice. **B and C,** p53 accumulation **(B)** and apoptosis 1 day after MI are reduced in CHIP-Tg mice. Apoptosis was assessed by cleaved PARP expression **(B)** and TUNEL staining **(C)**. Cleaved PARP level was assessed by densitometric analysis on band intensity of cleaved PARP over uncleaved PARP. $P<0.05$ vs WT; n=3. WT indicates wild-type mice. **D and E,** Postinfarct cardiac remodeling is attenuated in CHIP-Tg mice (n=15). HW/BW ratio **(D, left)**, contractile function **(D, right)**, and percentage fibrotic area **(E)**. *$P<0.01$ vs WT (n=30).

and less ventricular remodeling (Figure 6C and 6D). Interestingly, the effects of 17-AAG were greater than CHIP overexpression (compare Figures 5 and 6), suggesting that 17-AAG possesses cardioprotective activities that do not involve CHIP-mediated p53 degradation. As protein stability of cardioprotective proteins such as Hsp70 and HSF-1 was increased in vitro (Online Figure IV, B and C), we have examined the expression of these proteins in 17-AAG–treated mice. As expected, expression of these two proteins were increased by 17-AAG treatment (Online Figure IV, D), indicating that 17-AAG exerts its antiapoptotic effects by at least two mechanisms, one by inducing CHIP-mediated p53 degradation and the other by increasing cardioprotective heat shock proteins.

Finally, we examined the contribution of CHIP-mediated p53 degradation on the cardioprotective effects of 17-AAG. For that purpose we used CHIP heterozygous mice. There were no differences in cleaved PARP level (Figure 7A; compare WT Sham and Het Sham) or cardiac function between CHIP heterozygous mice and wild-type littermates at the basal level (Table). Following coronary artery ligation, however, apoptotic cell death was observed more prominently in CHIP heterozygous mice as assessed by increased cleaved PARP level (Figure 7A; compare WT MI and Het MI) and increased TUNEL positive cells (Figure 7B). The level of p53 accumulation was comparable following myocardial infarction between wild-type and CHIP heterozygous mice, suggesting the presence of p53 independent mechanisms for enhanced apoptosis caused by CHIP haploinsufficiency. Chronically, CHIP heterozygous mice showed worse cardiac function and worse ventricular remodeling compared with wild-type mice (Figure 7C and 7D). 17-AAG treatment was less effective to reduce p53 protein level, cleaved PARP level (Figure 7A; compare Het MI and Het MI 17-AAG), and TUNEL positive cardiomyocytes in CHIP heterozygous mice, possibly as a result of CHIP haploinsufficiency. 17-AAG treatment had minimal effects on improvements of cardiac function and ventricular remodeling on CHIP heterozygous mice also in the chronic phase (Figure 7C and 7D).

However, we must emphasize that the effects of 17-AAG were not fully attributable to CHIP-mediated p53 degradation